Effects of Dissipation on Collective Behaviour in Circuit Quantum Electrodynamics

Felix Beat Fabian Nissen
Churchill College, University of Cambridge

This dissertation is submitted for the degree of Doctor of Philosophy

April 2013

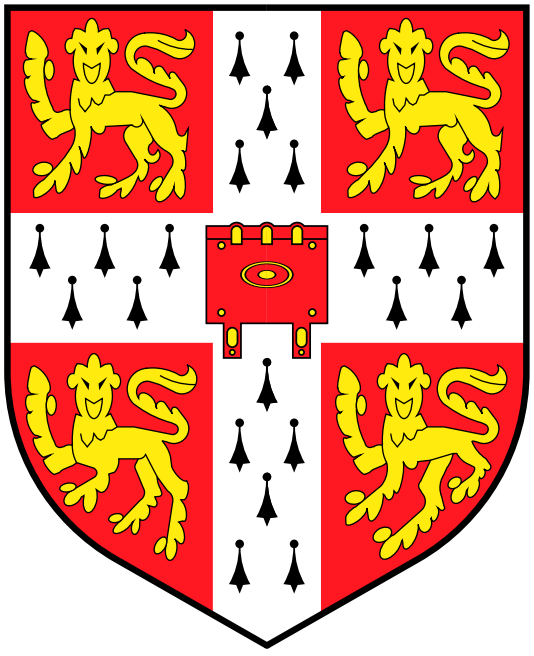

Contents

I Introduction **11**

1 Introduction and Background **13**

1.1 Quantum Optics 14

1.1.1 Quantising the Electromagnetic Field 14

1.1.2 Photon Statistics and Phenomena 16

1.2 Open Quantum Systems 18

1.2.1 Master Equation Approach 18

1.2.2 Keldysh Non-Equilibrium Path Integral Forumlation . 21

1.3 Time-Evolving Block Decimation 24

2 The Jaynes-Cummings Model **29**

2.1 Properties of the Jaynes-Cummings Model 29

2.2 Experimental Details and Circuit QED 34

3 The Jaynes-Cummings Hubbard Model **41**

3.1 Elementary Properties 42

3.2 Mean-Field Theory 43

3.3 Relationship with the Bose-Hubbard Model 46

II The Jaynes-Cummings-Hubbard Model **47**

4 The Extended Equlibrium Model **49**

5 Non-Equilibrium Mean-Field Theory **55**

5.1 Introduction to the JCHM with drive and dissipation 55

5.1.1 Existing Work . . . 56
5.2 Steady State Solution . . . 56
5.2.1 Numerical Calculation . . . 57
5.2.2 Small Hopping: A Spin-Chain Model . . . 59
5.2.3 Large Hopping: A Semi-Classical Model . . . 63
5.2.4 'Phase diagram' out of equilibrium . . . 64
5.3 mean-field theories and semi-classics . . . 64
5.4 Fluorescence Spectra . . . 66
5.4.1 Idea . . . 66
5.4.2 Numerical Calculation . . . 67
5.4.3 The Spin-Chain Model . . . 70
5.4.4 The Semi-Classical Model . . . 71

6 Keldysh Path Integral Formulation 73
6.1 Saddle point equation . . . 74
6.2 Fluctuations and luminescence . . . 78

7 Time-Evolving Block Decimation 81
7.1 Implementation . . . 81
7.2 Results . . . 82

III Linewidth Narrowing of Qubits in a Cavity 89

8 Several Qubits in a Cavity 91
8.1 approximation and secularisation procedure . . . 93
8.2 Implementation . . . 96
8.3 Results . . . 97
8.4 Scaling of peak height . . . 100
8.5 Appendix: Energy shift . . . 102

IV Concluding Remarks 105

9 Conclusion 107

The Fine Print

Statement of Originality This dissertation is entirely my own work and contains nothing which is the result of collaboration, except where stated in the acknowledgements and text.

Statement of Length Thankfully, this dissertation does not exceed 60,000 words in length.

Published Work Some of the results presented in this dissertation have been published in or submitted to the following journals:

- "Nonequilibrium Dynamics of Coupled Qubit-Cavity Arrays", published in *Physical Review Letters* [1]
- "Disordered driven coupled cavity arrays: Non-equilibrium stochastic mean-field theory", published in *Physical Review A* [2]
- "Collective Suppression of linewidth in circuit QED", accepted for publication in *Physical Review Letters* [3]

Notation We use natural units where the reduced Planck's constant $\hbar = 1$.

Summary This dissertation is a theoretical study of the effects of drive and dissipation in systems of quantum optics and circuit quantum electrodynamics. By confining photons to a small mode volume it is possible to enhance their coupling to matter degrees of freedom, generating composite light-matter quantum systems. Such systems are subject to dissipation,

both from escaping photons and relaxation of the matter degrees of freedom, leading to out-of-equilibrium effects.

While many of the fundamental concepts in this field were conceived in the context of atoms interacting with light, recent progress in engineering, manufacturing and controlling superconducting qubits embedded in on-chip resonators has opened a promising avenue for testing quantum optical models. Here, we study the effects of dissipation in two such models: The Jaynes-Cummings Hubbard model describing a lattice of coupled cavities containing two-level systems; and the dephasing dominated coupling of multiple two-level systems in a cavity.

The Jaynes-Cummings Hubbard model is studied out of equilibrium by applying a numerical mean-field decoupling approach. Analytical models are derived in appropriate limits, and Keldysh non-equilibrium path integrals as well as time-evolving block decimation calculations are used in order to explore effects beyond mean-field theory. The particular focus of this work is on the coherent photon field and photon fluctuations — both of which are experimentally accessible.

Motivated by recent experiments, this work also studies the effects of non-trivial $(1/f)$ noise on multiple two-level systems coupled strongly to a single cavity mode. By performing a perturbative Bloch-Redfield calculation it is shown that unexpected narrowing of the collective Rabi peaks occurs when the dissipation has a strong dephasing component.

Acknowledgements

I have had the privilege of initially local and later remote supervision by Dr Jonathan Keeling, to whom I am grateful for his advice, ideas and support. It has been both educational and enjoyable to work under his patient guidance during the last few years.

A number of people have contributed to this work through advice, ideas and guidance, as well as technical and administrative support. I am grateful for collaborative publications to Dr Sebastian Schmidt, Prof. Hakan Türeci, Prof. Gianni Blatter, Dr Johannes Fink and Prof. Andreas Wallraff; for conversations and references to my second supervisors Prof. Ben Simons and Prof. Peter Littlewood; for ideas and discussions to Dr Richard Brierley, Dr Paul Eastham, Dr Alex Chin, Dr Alex Silver and (~~soon~~-to-be-Dr) Gen Zhang; for computing support to Dr Michael Rutter and Dr Daniel Corbett; for the telling of fairy tales as well as a thoroughly realistic world view to Prof. David Khmelnitskii; and for administrative support to Tracey Ingham, Helen Verrechia and David Taylor.

The last forty-two months have taught me not only the art of doing science, but also a number of skills transferable to the *real world*. Physical strength, and a realistic assessment of my lack thereof, were the result of climbing with (still-not-a-Dr) Gen Zhang, Dr Andrea Fischer, Dr Priyanka Seth and, on occasion, Marianne Bauer. Further credit is due to the latter two for polishing my communication skills in their capacity as my long-term office mates. The sharpening of my verbal reasoning, including the creation of neologisms, was largely thanks to cryptic crosswords undertaken during lunch breaks with Dr Daniel Cole and William Belfield. On the same occasions I somewhat involuntarily familiarised myself with Dr Michael Rutter's

view of English geography and the Conservative party of 1979-1990. Fostering my creativity and the development of taste buds worthy of ninety months in Cambridge were greatly aided by competitive wine tasting encouraged by Hannah Price. Felicitas Beichert was tremendously helpful with my re-acquisition of the German language as well as the appreciation of good food and whisky. Justyna Cwik helped with the eating and drinking thereof. Padding of my curriculum vitæ was provided by my membership and presidency of my college's graduate student committee, thanks to the support and encouragement of several friends.

Additionally, I am grateful for Christopher Berry's sense of humour, Stephanie Hill's unofficial minutes and her hospitality in the District of Columbia, Claire Fetherstonhaugh's official minutes and personal insights, Simona Lipstaite's boss's cat, and her hospitality and visits, Kaleen Gallagher's politics and vegetarian burgers, Carl Sequeira's laugh, company and sofa, Dr Priyanka Seth's attempts to teach me to swim faster and literally stretch further and Mr Gen Zhang's *encouragement* immediately prior to our PhD interviews.

A number of friends, in college and elsewhere, have been an invaluable source of energy, as have my family. I am particularly grateful to Leanne Sheen for her strong support and for aiding my escape from the bubble.

During the completion of this thesis I was supported financially by the Engineering and Physical Sciences Research Council. I am grateful for travel grants from the Institute of Physics, Churchill College, the POLATOM network and the Singapore School of Physics. The University of St Andrews generously provided regular trips to Scotland. This work was helped by Gaggia and Illy and generously hindered by Pol Roger and Bollinger.

Preface

The interaction of light and matter is an established [4, 5], yet still active field of research. By confining photons to a small mode volume, it is possible to study the quantum mechanics of composite light-matter systems. Although a great deal of experimental effort has gone into minimising dissipation, that is relaxation and decoherence of the matter part and the escape of photons, quantum optical systems are still fundamentally dissipative and hence display non-equilibrium physics.

This dissertation studies two aspects of the open system character of quantum optics: First we study the coherence properties and fluctuations of a lattice model of optical cavities containing two-level systems, the Jaynes-Cummings Hubbard Model. We apply mean-field, non-equlibrium Keldysh and time-dependent density matrix renormalisation group calculations in order to explore the relevant quantities in different limits. Secondly we investigate the seemingly simpler system of several two-level systems coupled to a single photon mode. Motivated by experimental results on qubits in microwave resonators, we study the effect of $1/f$ noise dephasing the two-level systems. These non-trivial fluctuations show the strong coupling nature of the quantum optical system with clear signatures in the optical transmission spectra.

While many of the fundamental concepts in this field were conceived in the context of atoms interacting with light, recent progress in engineering, manufacturing and controlling superconducting qubits embedded in on-chip resonators has opened a promising avenue for testing quantum optical models. We will therefore also review the key aspects of qubit design and experiments on microwave resonators.

Part I

Introduction

Chapter 1

General Introduction and Background

One of the most interesting topics of current research is the interface of condensed matter physics and quantum optics. While the former studies the properties of large composite systems with interactions between their constituents, particularly in thermodynamic equilibrium, the latter concerns itself with the interaction of small quantum objects and photons. It studies open, inherently non-equilibrium systems.

The interface of these two seemingly different fields — building large condensed matter systems out of quantum optical components, or equivalently constructing macroscopically large quantum optical systems — is where many interesting phenomena may be studied. What effects of each of the fields survive as one crosses over into the other? Where and how might one observe these effects experimentally?

The latter question is partially answered by the advent of superconducting qubits that couple strongly to on-chip microwave cavities. The necessary building blocks now exist and are just getting reliable enough. This leaves the theoretical understanding to be built up, which this thesis attempts to contribute to.

We will fundamentally address two questions:

1. The Jaynes-Cummings-Hubbard model [6], which describes a lattice of

coupled cavities containing a two-level system each, has been studied in detail in thermal equilibrium. What happens if drive and dissipation are added to the model?

2. In strongly coupled light-matter systems, in particular in the context of superconducting qubits in a solid state environment, the role of dissipation may be a complex one [7, 8]. What happens if a strongly coupled light-matter system experiences frequency-dependent noise?

We start by introducing the relevant concepts and tools necessary to understand existing work in Part I before attempting to answer these questions.

In Part II we will investigate the collective behaviour of the Jaynes-Cummings-Hubbard model out of equilibrium. Part III studies the effect of noise on strongly coupled quantum optical systems. In order to understand both, we will review the quantisation of the electromagnetic field; the simplest of quantum optical models, the Jaynes-Cummings model; and the relevant concepts and quantities necessary to study the quantum mechanics of the systems we are interested in. We will also summarise existing tools and results about open quantum systems; and possible experimental realisations. Part I introduces the relevant concepts and reviews existing work. Parts II and III contain the original work presented in this thesis.

1.1 Quantum Optics

1.1.1 Quantising the Electromagnetic Field

Quantum optics studies the interaction of quantum mechanical light and matter, which requires a way to quantise light fields. Starting from the classical electromagnetic vector potential $\mathbf{A}(\mathbf{r}, t)$, we briefly review the quantisation of electromagnetism in free space, following [9].

In the Coulomb gauge $\nabla \cdot \mathbf{A}(\mathbf{r}, t) = 0$, the wave equation

$$\nabla^2 \mathbf{A}(\mathbf{r}, t) = \frac{1}{c^2} \partial_t^2 \mathbf{A}(\mathbf{r}, t) \tag{1.1}$$

can be re-phrased as an ordinary differential equation by Fourier transformation

$$\left(\nabla^2 + \frac{\omega_k^2}{c^2}\right)\mathbf{u}_k(\mathbf{r}) = 0 \tag{1.2}$$

$$\mathbf{A}(\mathbf{r},t) = \mathbf{A}^+(\mathbf{r},t) + \mathbf{A}^-(\mathbf{r},t) \tag{1.3}$$

$$\mathbf{A}^+(\mathbf{r},t) = \sum_k c_k \mathbf{u}_k(\mathbf{r}) e^{-i\omega_k t}. \tag{1.4}$$

c_k are the Fourier components, the mode functions $\mathbf{u}_k(\mathbf{r})$ are orthonormal and one may re-cast the full vector potential in the form

$$\mathbf{A}(\mathbf{r},t) = \sum_k \sqrt{\frac{\hbar}{2\omega_k\epsilon_0}}\left(a_k\mathbf{u}_k(\mathbf{r})e^{-i\omega_k t} + a_k^*\mathbf{u}_k^*(\mathbf{r})e^{i\omega_k t}\right). \tag{1.5}$$

By imposing bosonic commutation relations $[a_k, a_k^\dagger] = 1$ for the Fourier components, the Hamiltonian $H = \frac{1}{2}\int \mathrm{d}\mathbf{r}\ (\epsilon_0\mathbf{E}^2 + \mu_0\mathbf{H}^2)$ can be re-written in terms of photon creation and annihilation operators as

$$H = \sum_k \hbar\omega_k\left(a_k^\dagger a_k + \frac{1}{2}\right). \tag{1.6}$$

The two most common representations of photon states follow immediately from this quantisation procedure. The most obvious basis, in which photon states may be expressed, is the set of number or *Fock* states. The Fock state $|n_k\rangle$ contains n_k photons in mode k,

$$|n_k\rangle = \frac{(a_k^\dagger)^{n_k}}{\sqrt{n_k!}}|0\rangle. \tag{1.7}$$

As Fock states contain a fixed (usually small) number of photons, these are very quantum mechanical states with a large uncertainty in phase. By combining all number states in the form of a Poisson distribution, the joint uncertainty in phase and number can be minimised (corresponding to the limiting

case of the uncertainty principle[1]), giving the coherent state description

$$|\alpha\rangle = e^{-|\alpha|^2/2} \sum_n \frac{\alpha^n}{\sqrt{n!}} |n\rangle. \tag{1.8}$$

These are the most classical states.

Interactions between light and matter may be added to this description by postulating a minimum coupling Hamiltonian $\frac{1}{2m}(\mathbf{p} - q\mathbf{A})^2$ and re-writing the linear term $\propto \mathbf{p} \cdot \mathbf{A}$ in terms of a dipole operator. Using a dipole approximation and neglecting quadratic terms in $\mathbf{A}$ for small values of the field, this gives rise to the famous Jaynes-Cummings model, which is described in many standard texts. We will, however, arrive at this model in the context of circuit quantum electrodynamics as described in Chapter 2.2.

1.1.2 Photon Statistics and Phenomena

Photon Bunching and Anti-Bunching

One of the most interesting questions one may ask about quantised light is that of correlations between photons. These are expressed through correlation functions such as the normalised second-order correlation function (see, e.g. [9])

$$g^{(2)}(t=0) = \frac{\langle a^\dagger a^\dagger a a \rangle}{\sqrt{\langle a^\dagger a \rangle \langle a^\dagger a \rangle}} \tag{1.9}$$

$$= 1 + \frac{\sigma^2 - \langle n \rangle}{\langle n \rangle^2} \tag{1.10}$$

where σ^2 is the variance of the photon distribution and $\langle n \rangle$ is the mean. $t = 0$ indicates that we are studying the correlations between photons at the same point in time.

It is thus clear that there are fundamentally two different regimes: 1. When the variance is larger than the mean, $g^{(2)} > 1$. This corresponds to

[1] The limiting case of the uncertainty principle is realised by a set of so-called *squeezed states* that are formed by deforming the phase space distribution of the coherent state while preserving the uncertainty.

situations found in classical electrodynamics. 2. When the variance in photon number is smaller than the mean, $0 \leq g^{(2)} < 1$, and the light is quantum mechanical; this situation cannot be achieved with purely classical light. The coherent state with $g^{(2)} = 1$ forms the boundary between these two regimes and is the most quantum mechanical of classical states (or equivalently the most classical of the quantum mechanical states).

In the case where $g^{(2)} > 1$, we speak of 'bunching'. This term is based on the observation of the correlated emission of photons where the detection of a single photon makes it *more* likely to detect another one at the same time. When $g^{(2)} < 1$ ('anti-bunching') the detection of a photon makes a second detection *less* likely.

The Quantum Regression Theorem

In addition to $g^{(2)}$, we will be interested in the spectral information of quantum optical systems contained in the Fourier transform of the correlation function $\langle a^\dagger(t)a(0)\rangle$. The Quantum Regression Theorem [10, 11] provides a convenient way of simplifying the calculation of such correlation functions.

Given a two-time correlation function $\langle B(t)A(0)\rangle$ between two operators A and B, we can perform cyclic permutations of operators under the trace. Noting that system operators only act on the system Hilbert space, and defining the unitary time evolution operators $U(t)$, $U^\dagger(t)$, we find that

$$\begin{aligned}
\langle B(t)A(0)\rangle &= \mathrm{tr_S}\,\mathrm{tr_R}\left(U^\dagger(t)B(0)U(t)A(0)\rho_S(0)\otimes\rho_R(0)\right) && (1.11)\\
&= \mathrm{tr_S}\,\mathrm{tr_R}\left(B(0)U(t)A(0)\rho_S(0)\otimes\rho_R(0)U^\dagger(t)\right) && (1.12)\\
&= \mathrm{tr_S}\left(B(0)\mathrm{tr_R}\left(\left[A(0)\rho_S(0)\right](t)\otimes\rho_R(t)\right)\right) && (1.13)\\
&= \mathrm{tr_S}\left[B(0)\rho_S(t)\right]_{\rho_S^{\mathrm{initial}}\to A(0)\rho_S}. && (1.14)
\end{aligned}$$

In the third line we have made use of the factorisability of the system and bath density matrices (ρ_S and ρ_R) as based on the Born-Markov approximation discussed in section 1.2.1. The last line states the quantum regression theorem: Calculating the original two-time correlation function is equivalent to calculating the expectation value of the original operator B using the sys-

tem density matrix at time t, subject to an initial condition $A(0)\rho_S(0)$ at time 0. We will use the quantum regression theorem in conjunction with the Wiener-Khintchine theorem in order to calculate the fluorescence spectrum of a quantum optical system. As pointed out by [11], the quantum regression theorem requires the reservoir(s) to be unchanged by the perturbation $A(0)\rho_S$. As mentioned above, it only applies to Markovian systems.

1.2 Open Quantum Systems

1.2.1 Master Equation Approach

The systems we are dealing with typically contain some matter degrees of freedom, such as internal states of atoms or the discrete energy levels of a superconducting qubit, coupled to a (cavity-)confined photon mode. Not only do photons leak out of the cavity in any real experiment, but the matter degrees of freedom also experience forms of dissipation.

In general the dissipation associated with both photons and two-level systems, which we will use to represent the matter degrees of freedom, is caused by coupling the relevant system operators to a reservoir environment. In general all forms of dissipation can be described by the full density matrix of the system and the reservoir inducing the dissipation. However, when the coupling between the system of interest and the reservoir is weak, it is more useful to find an effective description of the dissipation in terms of system operators and parameters such as reservoir occupation functions.

The full density matrix can be written as a tensor product,

$$\rho(t) = \rho_S(t) \otimes \rho_R(t), \tag{1.15}$$

and follows the von Neumann equation of motion,

$$\frac{\mathrm{d}}{\mathrm{d}t}\rho(t) = -i\,[H, \rho(t)] \tag{1.16}$$

However, if we only calculate expectation values within the Hilbert space of the system, the density operator of interest is that of the system alone

obtained by partial trace

$$\rho_S(t) = \mathrm{tr}_R\left[\rho(t)\right]. \tag{1.17}$$

In finding the system-only equation of motion for $\rho_S(t)$, we follow the standard treatment, see e.g. [12]. With the Hamiltonian composed of system (S) and reservoir (R) parts as well as an interaction (SR) between them, $H = H_S + H_R + H_{SR}$, and transforming to the interaction picture, the equation of motion becomes

$$\tilde{\rho}(t) = -i\int^t \mathrm{d}t' \left[\tilde{H}_{SR}(t'), \tilde{\rho}_{SR}(t')\right] \tag{1.18}$$

after formal integration. Using the von Neumann equation again, the system density operator satisfies

$$\frac{\mathrm{d}}{\mathrm{d}t}\tilde{\rho}_S(t) = -\mathrm{Tr}_R\int^t \mathrm{d}t' \left[\tilde{H}_{SR}(t), \left[\tilde{H}_{SR}(t'), \tilde{\rho}_{SR}(t')\right]\right]. \tag{1.19}$$

At this point we assume that:

- The density operator of the reservoir is time-independent, $\tilde{\rho}_R(t) = \tilde{\rho}_R(0)$.

- $\tilde{\rho}_S(t') = \tilde{\rho}_S(t)$, which corresponds to a dense spectrum of bath modes leading to delta functions in time. This effectively means that the change in the system density operator depends on the current state of the system, but not on its entire history.

- The correlations are small enough for the approximation $\tilde{\rho}_{SR}(t') = \tilde{\rho}_S(t') \otimes \tilde{\rho}_R(t')$ to hold.

These assumptions constitute the Born-Markov approximation and allow us to simplify equation (1.19):

$$\frac{\mathrm{d}}{\mathrm{d}t}\tilde{\rho}_S(t) = -\mathrm{Tr}_R\int^t \mathrm{d}t' \left[\tilde{H}_{SR}(t), \left[\tilde{H}_{SR}(t'), \tilde{\rho}_S(t) \otimes \tilde{\rho}_R(0)\right]\right]. \tag{1.20}$$

This result is a second-order perturbative effect exerted on the system because of the coupling to reservoirs.

For example, a photon mode may be described by

$$\begin{aligned} H_S &= \omega a^\dagger a \\ H_R &= \sum_i \omega_i b^\dagger b \\ H_{SR} &= \sum_i g_i \left(a^\dagger b_i + a b_i^\dagger \right) \end{aligned} \tag{1.21}$$

with bosonic a and bath modes $\{b_i\}$. Imparting a time dependence $\xi_i = e^{i(\omega-\omega_i)(t-t')}$ by transforming into the interaction picture, we obtain

$$\begin{aligned} \frac{\mathrm{d}}{\mathrm{d}t}\tilde{\rho}_S(t) = -\sum_i |g_i|^2 \int^t \mathrm{d}t' \Big[&\left(a a^\dagger \langle b_i^\dagger b_i \rangle \xi_i + a^\dagger a \langle b_i b_i^\dagger \rangle \xi_i^* \right) \tilde{\rho}_S(t) \\ &- \left(a \tilde{\rho}_S(t) a^\dagger \langle b_i b_i^\dagger \rangle + a^\dagger \tilde{\rho}_S(t) a \langle b_i^\dagger b_i \rangle \right) (\xi_i + \xi_i^*) \\ &+ \tilde{\rho}_S(t) \left(a a^\dagger \langle b_i^\dagger b_i \rangle \xi_i^* + a^\dagger a \langle b_i b_i^\dagger \rangle \xi_i \right) \Big] . \end{aligned} \tag{1.22}$$

If there is a smooth density of states, the sum over exponential time dependences will turn into a sum over delta functions in time. Assuming empty decay baths, the system density matrix then satisfies

$$\frac{\mathrm{d}}{\mathrm{d}t}\tilde{\rho}_S(t) = \frac{\kappa}{2} \left(2 a \tilde{\rho}_S(t) a^\dagger - a^\dagger a \tilde{\rho}_S(t) - \tilde{\rho}_S(t) a^\dagger a \right) \tag{1.23}$$

where the decay rate κ depends on the coupling constants to bath modes $\{g_i\}$. The right-hand side is a Lindblad decay operator, which we write as

$$\mathcal{L}[a] = 2 a \rho a^\dagger - a^\dagger a \rho - \rho a^\dagger a, \tag{1.24}$$

dropping the explicit time-dependence and reference to the interaction picture. Similar decay terms may be found for the relaxation of two-level systems ($\mathcal{L}[\sigma^-]$ in Pauli matrix notation) and other dissipative processes. As discussed in [13], the Lindblad operator form is the only time-independent form of the decay term that preserves positivity of the density matrix.

It is crucial to note that we have assumed a dense spectrum and a flat, smooth density of states in addition to the Born-Markov approximation. This gives rise to decay rates that are independent of the system Hamiltonian. As we will see in Part III, this is not always true.

1.2.2 Keldysh Non-Equilibrium Path Integral Forumlation

In Part II we will be studying the non-equilibrium physics of a lattice model. Such models are common in condensed matter physics where the technique of Keldysh non-equilibrium path integrals was developed [14].

In equilibrium systems one can describe the entire physics by finding the full set of energy eigenstates. Once the spectrum is known, one can calculate the desired thermodynamic properties from the partition function. The occupation of the spectrum is given by fluctuation-dissipation relations and is fully determined once the energy eigenstates are known. Out of equilibrium, however, the spectrum and its occupation are distinct quantities — properties such as drive and decay rates determine the occupation of states. Rather than calculating a single Green function (i.e. a single correlation function between system operators), it is necessary to determine two linearly independent Green functions in the case of a non-equilibrium system.

Excellent reviews of the Keldysh path integral formalism and its applications in condensed matter and quantum optical systems already exist [15–17]. Here, we will discuss the main ideas and amalgamate the crucial points made in these references into a brief introduction.

When studying many-body quantum systems, one is usually interested in time-ordered correlation (Green) functions of the form

$$iG_\phi\left(x,t,x',t'\right) = \langle\phi|\mathrm{T}\left[A(x,t)B(x',t')\right]|\phi\rangle \tag{1.25}$$

from which the full correlation function $G = \sum_\phi p_\phi G_\phi$ may be calculated. The Heisenberg picture states $|\phi\rangle$ define the density operator $\rho = \sum_\phi p_\phi |\phi\rangle\langle\phi|$.

Using the time-dependent part of the Hamiltonian in the interaction picture[2] $\tilde{H}(\tau)$, we can define the time-ordered propagator

$$S_{t,t'} = \mathrm{T} \exp\left(-i \int_{t'}^{t} \mathrm{d}\tau \tilde{H}(\tau) \right). \tag{1.26}$$

The correlation function then takes the form

$$\begin{aligned} i \quad & G_\phi(x,t,x',t') && (1.27)\\ = \quad & \langle \phi^I_\infty | S_{\infty,0} \mathrm{T}\left[S_{0,t} A(x,t) S_{t,t'} B(x',t') S_{t',0} \right] S_{0,-\infty} | \phi^I_{-\infty} \rangle && (1.28)\\ = \quad & \langle \phi^I_\infty | \mathrm{T}\left[S_{\infty,-\infty} A(x,t) B(x',t') \right] | \phi^I_{-\infty} \rangle. && (1.29) \end{aligned}$$

$|\phi^I_t\rangle$ is the original Heisenberg picture state $|\phi\rangle$ transformed to the interaction picture at time t. The last line simply follows from combining all time-ordering operations into a single one.

So far we have simply followed the Feynman path integral description of quantum mechanics. Equation (1.29) now shows why this is bound to fail in non-equilibrium systems: In the next step we would ordinarily argue that the interactions are switched on (off) adiabatically in the distant past (future). For the ground state the adiabatic theorem ensures that the initial and final states are the same up to a phase factor e^{iL}. For excited states and out of equilibrium, however, the final state may well be more complex as the time evolution of any non-trivial problem is non-adiabatic and is almost certainly unknown.

In order to get around this issue, one can introduce the Schwinger[18]-Keldysh[14] contour. Once we have integrated along the time axis from $-\infty$ to ∞ we can avoid the final state by integrating backwards in time until we return to the initial state at $t = -\infty$, allowing the fields along the backward portion of the integration path to differ from those along the forward branch. This solves the final state problem, but comes at the cost of doubling the number of degrees of freedom. Unlike in equilibrium, however, occupation

[2] i.e. the interacting part of the Hamiltonian that acquires a time-dependence in the interaction picture

and spectrum are not related by a fluctuation-dissipation theorem, which doubles the amount of information necessary to fully describe the system. This requirement can be satisfied by calculating two linearly independent Green functions. By deriving an action from a set of system, bath and interaction Hamiltonians one can then perform a saddle point analysis in order to find a mean-field equation and use correlation (Green) functions to describe fluctuations about the saddle point. The Keldysh technique is thus analogous to the diagrammatic Feynman approach known from equilibrium physics.

Even for equilibrium theories non-adiabadicity can be present. The usual solution in equilibrium is to either restrict one's analysis to ground states (as in high energy physics), or to use the partition function in thermal equilibrium, $Z = \mathrm{tr}\exp(-\beta H)$. This quantity is directly accessible via Matsubara summation with periodic or anti-periodic boundary conditions, avoiding the issue of having to deal with Keldysh path integrals.

In Part II we will be studying coherence properties of a quantum optical many-body (lattice) system. Two linearly independent Green functions are sufficient to describe the energy levels and occupation. Labelling fields on the forward and backward branches of the closed-time contour as $\psi_{\mathrm{f,b}}$ respectively, we define 'classical' and 'quantum' field operators $\psi_{\pm} = (\psi_{\mathrm{f}} \pm \psi_{\mathrm{b}})/\sqrt{2}$. The full set of bosonic Green functions (retarded, advanced and Keldysh) is defined as [19]

$$D = \begin{pmatrix} D^K & D^R \\ D^A & 0 \end{pmatrix} \tag{1.30}$$

$$= -i \left\langle \mathrm{T_C} \begin{pmatrix} \psi_+(x,t) \\ \psi_-(x,t) \end{pmatrix} \begin{pmatrix} \psi_+^\dagger(x,0) & \psi_-^\dagger(x,0) \end{pmatrix} \right\rangle \tag{1.31}$$

with $\mathrm{T_C}$ denoting ordering along the closed time contour. It follows from

$D^{-1}D = I$ that

$$D^{-1} = \begin{pmatrix} 0 & \left[D^A\right]^{-1} \\ \left[D^R\right]^{-1} & \left[D^{-1}\right]^K \end{pmatrix} \tag{1.32}$$

$$= \begin{pmatrix} 0 & \left[D^A\right]^{-1} \\ \left[D^R\right]^{-1} & -\left[D^R\right]^{-1} D^K \left[D^A\right]^{-1} \end{pmatrix}. \tag{1.33}$$

As described above we may define the path integral as a closed-contour path integral over bosonic (ψ_i) and fermionic (ϕ_j) system and bath modes,

$$Z \propto \int \prod \mathcal{D}\psi_i \prod \mathcal{D}\phi_j \, \mathrm{e}^{iS}. \tag{1.34}$$

The action S is given by

$$S = \int_C \mathrm{d}t \sum_i \bar{\psi}_i \left(i\partial_t - \omega_i\right) \psi_i + \ldots \tag{1.35}$$

with the exact form depending on the modes involved as well as their interactions. In Chapter 6 we will use this approach to describe the driven, dissipative Jaynes-Cummings Hubbard model.

1.3 Time-Evolving Block Decimation

In dealing with collective quantum phenomena, we face the problem of an exponentially large Hilbert space: Given a lattice model consisting of building blocks with a d-dimensional Hilbert space, the full system of N building blocks requires us to solve a d^N-dimensional problem. Even numerically this is often too big to solve, making appropriate approximation schemes necessary.

In one dimension a suitable approximation scheme was introduced by Steven White [20]: the density-matrix renormalisation group (DMRG). A chain of coupled quantum systems is split into pairs of adjacent sites. Numerically diagonalising the two site density matrices of each of these two-site blocks, only the most relevant (biggest) eigenvalues are retained. Itera-

tively, the overall collective ground state emerges while only retaining a small Hilbert space.

This method has been applied successfully to antiferromagnetic Heisenberg chains [20] and other one-dimensional problems. The reason for its accuracy is the scaling of quantum entanglement. Splitting a lattice into two regions A and B, the entanglement between these regions is expected to scale as the surface area between them. However, in one dimension this surface area is constant. As a result, it is possible to capture the relevant quantum physics in a small number of eigenvalues describing the entanglement between any two sites.[3]

A time-dependent version of the DMRG method, frequently known as time-evolving block decimation (TEBD), was introduced by [22–25] for pure quantum states and later extended to mixed-state dynamics [26]. Both are formulated in terms of matrix product states.

Consider an arbitrary pure state of a two-site system. A d-dimensional Hilbert space is associated with each site. The basis states $\{|i\rangle_A, |j\rangle_B\}$ are entangled by a matrix c of coefficients

$$|\psi\rangle = \sum_{i,j}^{d} c_{ij}|i\rangle_L \otimes |j\rangle_R. \tag{1.36}$$

However, a singular value decomposition of c yields two Hermitian matrices U, V and a non-negative (real) diagonal one Λ,

$$c = U\Lambda V^\dagger \tag{1.37}$$

such that the full state can be written in terms of re-defined single site states as

$$|\psi\rangle = \sum_{ij}^{d}\sum_{k}^{d} \Lambda_{kk}\left(U_{ik}|i\rangle_L\right) \otimes \left([V^\dagger]_{kj}|j\rangle_R\right). \tag{1.38}$$

The singular values $\{\lambda_k \equiv \Lambda_{kk}\}$ then describe the entanglement between the

[3]Exceptions may apply in the case of gapless spectra or criticality, where logarithmic corrections are possible [21].

two sites as

$$\begin{aligned} |\psi\rangle &= \sum_{k}^{d} \lambda_k \left(\sum_i U_{ik} |i\rangle_L \right) \otimes \left(\sum_j [V^\dagger]_{kj} |j\rangle_R \right) \\ &= |\psi_A\rangle \Lambda |\psi_B\rangle \end{aligned} \tag{1.39}$$

where $|\psi_A\rangle$ and $|\psi_B\rangle$ are row and column vectors of (complex) rotated basis states. We hence see how one may describe the entanglement between two d-dimensional quantum systems as a non-negative (real) diagonal matrix. This decomposition procedure is also known as Schmidt decomposition [27].

Expressing an N-site state in terms of local basis states,

$$|\psi\rangle = \sum_{i,j,\ldots} c_{ijk\ldots} |i\rangle \otimes |j\rangle \otimes \ldots \tag{1.40}$$

we can bipartition the lattice in an arbitrary position L and represent the entanglement between the d^L-dimensional left-hand part and the d^{N-L}-dimensional right-hand part by a $\min(d^L, d^{N-L})$-dimensional diagonal matrix of singular values. By repeating this decomposition across the one-dimensional lattice, the rank-N tensor c becomes

$$c_{i_1 i_2 \ldots} = \Gamma^{i_1} \Lambda^1 \Gamma^{i_2} \Lambda^2 \ldots \Gamma^{i_N} \tag{1.41}$$

with i_α labelling the ith basis state at site α. The Γ matrices represent the on-site states, whereas the Λs act as *bonds* between adjacent sites. These are just the singular values arising from Schmidt decompositions.

The fundamental idea of the TEBD algorithm is now to truncate the size of the Γ and Λ matrices: As we expect the entanglement in a one-dimensional system to be small, only a small number χ of dimensions per *bond* need to be retained in order to capture the physics. Numerical studies suggest that the singular values decrease exponentially [24].

The kinds of operators we might want to apply to matrix product states usually involve up to two sites — e.g. interactions between adjacent sites. Given an operator $P = \sum_{i_L i_{L+1} j_L j_{L+1}} \langle i_L i_{L+1} | P | j_L j_{L+1} \rangle | i_L i_{L+1} \rangle \langle j_L j_{L+1} |$ in the

local bases of two adjacent sites, we have

$$P\,\Gamma^{i_L}\Lambda^L\Gamma^{i_{L+1}} = \sum_{j_L j_{L+1}} \langle i_L i_{L+1}|P|j_L j_{L+1}\rangle \Gamma^{j_L}\Lambda^L\Gamma^{j_{L+1}}. \tag{1.42}$$

By singular value decomposition, we can again represent this two-site state as a product $\Gamma^{i_L}\Lambda^L\Gamma^{i_{L+1}}$. In order to recover the matrix product state formulation where the Γ matrices are linked by i_L-independent bond matrices Λ^L, we consider the matrix of all $P\,\Gamma^{i_L}\Lambda^L\Gamma^{i_{L+1}}$ and only retain the χ largest singular values and associated Γs.

Given a Hamiltonian H, we can now solve the Schrödinger equation and obtain the time evolution. Dividing H into two-site operators, we can apply the propagator $P = \mathrm{e}^{iH_{L,L+1}t}$ separately for each pair of sites. As in general $[H_{L,L+1}, H_{L',L'+1}] \neq 0$ one may use the fact that

$$\mathrm{e}^{(F+G)t} = \mathrm{e}^{\frac{1}{2}Ft}\mathrm{e}^{\frac{1}{2}Gt}\mathrm{e}^{\frac{1}{2}Ft} + \mathcal{O}(t^3). \tag{1.43}$$

This is the second-order Suzuki-Trotter decomposition, which is an improvement over the second order error $\mathrm{e}^{(F+G)t} = \mathrm{e}^{Ft}\mathrm{e}^{Gt} + \mathcal{O}(t^2)$ one would otherwise incur from the Hausdorff-Baker-Campbell property. Given small time steps, one can hence obtain the approximate time-evolution by applying two-site propagators. In order to preserve physicality, the total wavefunction needs to be normalised at every time step, compensating for the singular values that were discarded.

Dimensionality and boundary conditions The Γ and Λ matrices are χ-by-χ matrices (*bond dimension* χ). However, for a lattice with two end points, the Γs at the end points have size 1-by-χ and χ-by-1, respectively. In order to avoid redundant degrees of freedom, the bond dimensions (which may vary between bonds) should be $\chi \leq d^L$ for a d-dimensional local Hilbert space at distance L from the nearest boundary. If one wishes to consider periodic boundary conditions, one may use a chain that 'terminates' in a Λ matrix, which wraps around to join up with the Γ on site 1. There is a known requirement for a modified update step, which is described in detail in [28].

Density Matrix Time-Evolution For open systems, mixed and thermal states, we need a description for the time evolution of the density matrix. In the case of an open quantum system the density operator ρ satisfies the von Neumann equation

$$\frac{\mathrm{d}}{\mathrm{d}t}\rho = -i[H,\rho] + \sum_i \mathcal{L}[a_i] \tag{1.44}$$

for some system operators a_i that are coupled to decay baths. Like the Schrödinger equation, this is a first-order ordinary differential equation in time. We can thus write the components of ρ as a vector $\rho_\#$ and define an effective (non-Hermitian) Hamiltonian $M^\#$

$$\frac{\mathrm{d}}{\mathrm{d}t}\rho_\# = M^\#\rho_\#. \tag{1.45}$$

The density matrix can then be written as a matrix product state and time-evolved in the same way. However we need to normalise the Γs at every step of the time evolution in order to preserve the total (physical) trace of 1 (rather than the norm of the state vector, which is ordinarily used as the normalisation condition in pure state problems). The TEBD procedure for density matrices truncates correlations, whereas the wavefunction version truncates entanglement. The application of TEBD to density matrices was first introduced by Zwolak and Vidal [26].

Chapter 2

The Jaynes-Cummings Model

Before we can explore the collective behaviour of extended quantum optical systems, we need to understand a single building block. First introduced in 1963 [29], the Jaynes-Cummings Model describes the interaction of a single quantum system with two discrete energy levels and a bosonic mode, such as a photon. It is possible to derive this model from microscopic physics in different contexts, most notably the dipole interaction of atoms with photons and the strong coupling of superconducting qubits to microwave resonator modes [30]. As most of the microscopic details are discussed in Sections 1.1.1 and 2.2, we shall merely postulate the model here in order to review the physical phenomena associated with it.

2.1 Properties of the Jaynes-Cummings Model

Customarily, the Jaynes-Cummings Hamiltonian is written as

$$H^{\mathrm{JC}} = \omega a^\dagger a + \frac{\epsilon}{2}\sigma^z + g\left(a\sigma^+ + a^\dagger\sigma^-\right) \tag{2.1}$$

in the Schrödinger picture. The first term describes a bosonic mode a at energy ω. The two discrete energy levels associated with the matter degrees of freedom are described by a Pauli matrix σ^z with the transition energy ϵ. The third term accounts for the coupling between the photon mode and the two-level system by transferring excitations between the two. In Parts II

and III we will only consider the near-resonant case where the lowest photon states are close to the transition energies of the matter degrees of freedom. For the case of a single Jaynes-Cummings model this corresponds to $\omega \approx \epsilon$.

It is easy to see that the Hamiltonian in equation (2.1) commutes with the number operator $N = a^\dagger a + \frac{1}{2}(\sigma^z + 1)$ and hence conserves the number of excitations.[1] As a result, one may find the eigenstates separately for each integer number of excitations in the system by diagonalising a 2-by-2 matrix. Heuristically, this gives rise to hybridisation of the photon and two-level system modes to form hybrid states known as upper and lower polaritons. While the vacuum state remains unchanged, the $n > 0$ excitation subspace is spanned by the vectors [29]

$$|n,+\rangle = \cos\vartheta|n,\downarrow\rangle - \sin\vartheta|n-1,\uparrow\rangle \tag{2.2}$$

$$|n,-\rangle = \sin\vartheta|n,\downarrow\rangle + \cos\vartheta|n-1,\uparrow\rangle \tag{2.3}$$

$$E_n^\pm = n\omega + \frac{\epsilon-\omega}{2} \pm \sqrt{\frac{(\epsilon-\omega)^2}{4} + ng^2} \tag{2.4}$$

$$\tan(2\vartheta) = \frac{2g\sqrt{n}}{\epsilon-\omega}. \tag{2.5}$$

$|n,\downarrow\rangle$ denotes a state of n photons and the 'down-spin' component of the Pauli matrix. $\pm$ indicates that the polariton states are connected to the symmetric and anti-symmetric hybridisations that arise in the resonant case $\omega = \epsilon$, where

$$|n,\pm\rangle = \left(|n,\downarrow\rangle \pm |n-1,\uparrow\rangle\right)/\sqrt{2} \tag{2.6}$$

$$E_n^\pm = n\omega \pm g\sqrt{n}. \tag{2.7}$$

[1] Equation (2.1) is frequently derived in a picture where the coupling is mediated by a dipole interaction $\propto E \cdot d$. As the electric field E in quantised form contains both raising and lowering operators, and as the dipole operator $d \propto \sigma^x$, this would ordinarily give rise to non-number conserving terms $a\sigma^-$ and $a^\dagger\sigma^+$. If one transforms to the interaction picture, these acquire a phase evolution at frequency $\omega + \epsilon$ significantly faster than the number conserving terms, which rotate at $\omega - \epsilon \approx 0$. The former set of terms is therefore dropped, which is called the *Rotating Wave Approximation*. The model obtained by keeping the non-number conserving terms, which may be necessary for large detuning or strong drive strengths [31], is known as the Rabi Model.

The resonant case hence displays a ladder of energy levels that is strongly anharmonic (non-linear) with energy splittings $2g\sqrt{n}$ and $\omega+g(\sqrt{n}-\sqrt{n+1})$.

An important consequence of this anharmonicity is the *photon blockade* effect [32, 33]. Suppose we induce transitions between two polariton states, say $|0\rangle \leftrightarrow |1,-\rangle$. In order to achieve a significant transition rate, we use near-resonant light of energy $\approx E_1^- - E_0$. The non-linearity of the polariton spectrum now ensures that all other possible transitions are significantly off resonance — only the states $|0\rangle$ and $|1,-\rangle$ gain a significant population. Once a single excitation has been added to the system, the addition of further excitations (e.g. promoting the system to the $|2,-\rangle$ state) is blockaded. The photon blockade property of the Jaynes-Cummings model has been widely used in exerimental and theoretical quantum optics [33, 34], and many of the results in Parts II and III rely on it.

While the Jaynes-Cummings model without dissipation has been shown to exhibit collapse and revival of Rabi oscillations [35], we will focus on the coherence and fluorescence properties in the presence of decay. As discussed in Chapter 1.2, we can incorporate the physics of photons escaping from the cavity confining the bosonic mode as well as relaxation of the two-level system by adding Lindblad terms to the phase evolution of the density matrix [36]

$$\frac{\mathrm{d}}{\mathrm{d}t}\rho = -i[H,\rho] + \frac{\kappa}{2}\mathcal{L}[a] + \frac{\gamma}{2}\mathcal{L}[\sigma^-]. \tag{2.8}$$

The photon mode is driven coherently at amplitude f and frequency μ in order to compensate for the loss of excitations:

$$H = H^{\mathrm{JC}} + f\left(a\mathrm{e}^{i\mu t} + a^\dagger \mathrm{e}^{-i\mu t}\right). \tag{2.9}$$

By means of the gauge transformation $H \to UHU^\dagger$, with $U = \mathrm{e}^{i\mu\left(a^\dagger a + \sigma^z/2\right)}$, the time dependence is eliminated. The structure of the Hamiltonian is unchanged except for $\omega \to \omega - \mu$, $\epsilon \to \epsilon - \mu$. For ease of notation, we will drop the $-\mu$ terms and adopt a convention where all energies are measured with respect to the pump frequency.

The driven Jaynes-Cummings Hamiltonian is hence

$$H = \omega a^\dagger a + \frac{\epsilon}{2}\sigma^z + g\left(a\sigma^+ + a^\dagger\sigma^-\right) + f\left(a + a^\dagger\right). \tag{2.10}$$

Recent experiments [33, 37] have focused on the properties of the Jaynes-Cummings model when driving the transition between the vacuum and the lowest polariton state, $|0\rangle \leftrightarrow |1,-\rangle$. Given resonance ($\omega = \epsilon$), the two states effectively form a two-level system. One can therefore project the driven dissipative Jaynes-Cummings model onto the two most relevant states, giving rise to an effective Hamiltonian

$$H_{\text{eff}} = \frac{\Delta}{2}\tau^z + \frac{1}{\sqrt{2}}f\tau^x \tag{2.11}$$

and re-scaled decay rates. $\Delta = \left(\omega + \epsilon - \sqrt{(\omega-\epsilon)^2 + 4g^2}\right)/2$ is the transition energy of the effective two-level system and $\{\tau\}$ are Pauli matrices. The effective model for weak drive f displays Lorentzian transmission $|\langle a\rangle|^2$ vs. pump frequency about both vacuum Rabi peaks at $\omega = \pm g$. As the drive amplitude $f/\sqrt{2}$ increases, it acts as a field splitting the transmission peak: Each of the Rabi peaks develops a doublet structure with $|\langle a\rangle|$ decreasing at $\omega = \pm g$ to form an *anti-resonance*. This behaviour, termed 'supersplitting' [34] or 'dressing of dressed states' [34, 38, 39] has been seen experimentally in superconducting qubits embedded in on-chip microwave resonators. This pump scheme is shown in figure 2.1.

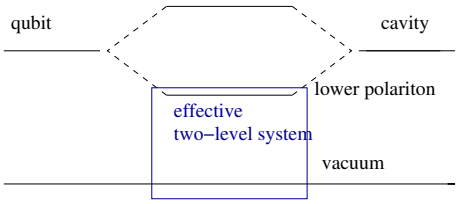

Figure 2.1: Schematic representation of the relevant energy levels of the Jaynes-Cummings model. The qubit and photon are resonant and hybridise to form upper and lower polariton states. The pump frequency is near the transition between the vacuum state and the lower polariton, which gives rise to an effective two-level system.

In addition to the expectation value of the photon operator, $|\langle a\rangle|$,[2] one may be interested in time-dependent quantum correlations. The simplest quantity describing such correlations is the spectrum of resonance fluorescence: Driving a two-level system coherently and resonantly, we are interested in calculating

$$\mathcal{S}(\omega) = 2\,\Re \int_0^\infty \mathrm{d}t \mathrm{e}^{i\omega t} \langle a^\dagger(t) a(0)\rangle_{\text{steady state}}. \tag{2.12}$$

By the Wiener-Khintchine Theorem, this is the emission spectrum [40, 41]. Using the Quantum Regression Theorem [11], this is equivalent to calculating

$$\mathcal{S}(\omega) = 2\,\Re \int_0^\infty \mathrm{d}t \mathrm{e}^{i\omega t} \langle a^\dagger(t)\rangle_{\rho'} \tag{2.13}$$

subject to the initial condition $\rho' = a(0)\rho_{\text{steady state}}$.[3] Using a Heisenberg equation, this can equivalently be written as [42]

$$\mathcal{S}(\omega) \propto 2\,\Re \int_0^\infty \mathrm{d}t \mathrm{e}^{i\omega t} \langle \sigma^+\rangle_{\rho'=\sigma^-\rho_{\text{steady state}}}. \tag{2.14}$$

Solving the von Neumann equation for this set of boundary conditions, $\mathcal{S}(\omega)$ exhibits a triplet structure of peaks of approximate weight ratios 1:2:1. This can be understood heuristically: The two-level system will hybridise with the n photon state to form two polariton states. Each of these can emit a photon into either of the two polariton states with $n-1$ excitations. There are thus four transition frequencies. For large n (i.e. large drive field), the transition frequencies are n-independent and two of them are the same, leading to the triplet structure. This is known as the Mollow triplet [43] and has been observed in circuit QED experiments [33].

[2]For details about the experimental set-up required to measure this quantity, refer to Chapter 2.2 or [37].

[3]Note that this assumes that the perturbation of the reservoir by the system is negligible and that the quantum regression theorem relies on the Markov approximation.

2.2 Experimental Details and Circuit QED

An interesting arena for studying quantum optics and open quantum systems is the field of circuit quantum electrodynamics (cQED). Rather than real atoms absorbing and emitting light, one can confine microwave radiation in resonators on dielectric chips. By placing carefully engineered superconducting qubits inside, one can achieve strong coupling between the discrete qubit energy levels and the radiation. Engineering and experimental control have reached the level where magnetic flux can be used to tune the qubit energy levels in resonance with the microwave resonator, making circuit QED a perfect setup for the experimental study of the Jaynes-Cummings model and the physics of related quantum (optical) models.

A superconducting qubit that has been used successfully to study Jaynes-Cummings physics [37] is the *transmon* qubit [44, 45].[4] Like in other superconducting qubits, phase coherence over a macroscopically large piece of superconductor is used to build a 'large' (macroscopic) quantum device — an object with a discrete energy spectrum — that is large enough to interact strongly with a confined microwave field.

In order to understand the engineering of the transmon qubit, let us review a simple Josephson junction (see e.g. [45]): Two superconducting islands are separated by a thin layer of insulating material. Cooper pairs can tunnel between the islands, giving rise to the phenomenological Hamiltonian in terms of Cooper pair number n,

$$H_J = -\frac{E_J}{2}\sum_n \left(|n\rangle\langle n+1| + |n+1\rangle\langle n|\right). \tag{2.15}$$

The Josephson energy E_J determines the tunnelling rate. The eigenstates of the Josephson Hamiltonian are the same as those of a tight-binding model,

$$|\phi\rangle = \sum_{n=-\infty}^{\infty} \mathrm{e}^{in\phi}|n\rangle \tag{2.16}$$

[4] This is essentially equivalent to the better-known Cooper pair box (CPB) operated at a much higher Josephson energy in order to reduce noise sensitivity [46].

which are plane wave states in the Cooper pair number space. The corresponding dispersion is [47]

$$H_J|\phi\rangle = -E_J \cos\phi|\phi\rangle. \tag{2.17}$$

Representing

$$|n\rangle\langle n+1| = \mathrm{e}^{-i\hat{\phi}}|n+1\rangle\langle n+1| \tag{2.18}$$

and promoting number and phase variables to canonically conjugate quantum operators $\{n, \phi\} \to \{\hat{n}, \hat{\phi}\}$, the Josephson Hamiltonian may be written as

$$H_J = -E_J \cos\hat{\phi}. \tag{2.19}$$

The simplest charge qubit, the Cooper pair box [46], uses a single Josephson junction. However, the same Hamiltonian with magnetically tunable E_J may be obtained by using a SQUID[5] setup where the two superconductors are linked by two Josephson junctions forming a magnetically threaded loop.[6] This latter setup is used for transmon qubits — a sketch of the original design is shown in figure 2.2.

In addition to the tunnelling energy, the number of Cooper pairs gives rise to a charging energy contribution

$$H_C = 4E_C\left(\hat{n} - n_g\right)^2 \tag{2.20}$$

where n_g is an offset charge defined by an external gate voltage and $E_C = \frac{e^2}{2C_{\mathrm{tot}}}$ with total capacitance C_{tot}. The transmon qubit can thus be described

[5] superconducting quantum interference device

[6] In this case, the Josephson Hamiltonian is the sum of two cosine terms $-E_J\left(\cos\hat{\phi}_1 + \cos\hat{\phi}_2\right)$ which, by means of a trigonometric identity, may be combined into a single term $-E_J\cos\left(\frac{\hat{\phi}_1+\hat{\phi}_2}{2}\right)\cos\left(\frac{\hat{\phi}_1-\hat{\phi}_2}{2}\right)$. The phase difference now acts as the canonical phase operator (as it only depends on the relative tunnelling of Cooper pairs through the two Josephson junctions). The sum of phases re-scales the amplitude of this (potential energy) term. Unlike the difference $\phi_1 - \phi_2$, the sum $\phi_1 + \phi_2$ is susceptible to magnetic flux through the loop enclosed by the Josephson junctions and one can use the latter to tune the effective Josephson energy, $E_J \to E_J\cos\left(\frac{\hat{\phi}_1+\hat{\phi}_2}{2}\right)$ [45].

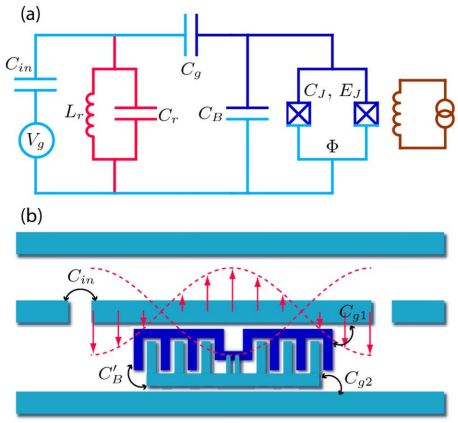

Figure 2.2: Sketch of the transmon qubit design taken from [30]. The two Josephson junctions (squares with crosses) are connected in a loop with a threaded magnetic flux ϕ used to tune the phase of the SQUID. Panel (a) shows the equivalent circuit of the physical setup in panel (b) where the transmon qubit is placed inside an on-chip transmission line resonator.

by

$$H = 4E_C \left(\hat{n} - n_g\right)^2 - E_J \cos\hat{\phi}. \tag{2.21}$$

Two standard approaches exist for finding the transmon eigenstates: We can represent the number operator as a canonically conjugate differential operator in ϕ-space, $\hat{n} = -i\partial_\phi$. In this case the eigenstates are the solutions to

$$\begin{aligned} 4E_C \left(-i\partial_\phi - n_g\right)^2 \boldsymbol{\psi}(\phi) - E_J \cos\phi\, \boldsymbol{\psi}(\phi) &= E\boldsymbol{\psi}(\phi) && (2.22) \\ \boldsymbol{\psi}(\phi + 2\pi) &= \boldsymbol{\psi}(\phi), && (2.23) \end{aligned}$$

which are Mathieu functions. The first (differential) term acts as a kinetic energy contribution of quantum motion in a periodic cosine potential. This suggests the second possible approach: For sufficiently large[7] E_J/E_C, the

[7] A design feature of transmon qubits is a small ratio E_J/E_C in order to minimise charge noise. However, the charge noise is suppressed exponentially, whereas the anharmonicity is algebraic, leaving a regime where both conditions may be satisfied [30]. The insensitivity to charge noise is achieved by biasing the qubit to a point where the charge dispersion has no slope, such that linear noise contributions do not change the transition frequencies.

effective potential $-E_J \cos\phi$ is approximately quadratic with a quartic (anharmonic) correction. The wavefunctions then no longer extend over the full period of $\phi \in [0; 2\pi]$, but only over a small part of it. As a result one may drop the periodicity condition (2.23) by defining wavefunctions on $(-\infty; \infty)$ which decay to zero at infinity. We can hence expect a discrete spectrum for the lowest energy levels that is almost harmonic, but not quite.

When embedded in a microwave resonator, the Cooper pairs couple to the resonator mode [44]:

$$H_{\text{coupling}} = 2\beta e V_{\text{rms}} \hat{n} \left(a + a^\dagger\right). \tag{2.24}$$

V_{rms} is the local oscillator voltage amplitude and β depends on the capacitances of the circuit. Absorbing some of the parameters into a set of coupling strengths

$$g_{ij} = 2\beta e V_{\text{rms}} \langle i|\hat{n}|j\rangle \tag{2.25}$$

and adding the bare photon (resonator) part, the total Hamiltonian of a resonator-transmon system becomes

$$H = \sum_j \epsilon_j |j\rangle\langle j| + \omega a^\dagger a + \sum_{ij} g_{ij} |i\rangle\langle j| \left(a + a^\dagger\right). \tag{2.26}$$

The sums run over transmon eigenstates. This is a Jaynes-Cummings Model with counter-rotating terms (Rabi model) generalised to include additional energy levels. It can be shown that $g_{ij} \to 0$ for $|i-j| \neq 1$ as $E_J/E_C \gg 1$ (i.e. only transitions between adjacent energy levels are supported by a significant matrix element). Additionally employing the Rotating Wave Approximation where only excitation number conserving transitions are allowed, one recovers the regular Jaynes-Cummings Model in a circuit QED setting by restricting the transmon states to two-level systems.

Experimental Design Being able to measure the quantities of theoretical interest directly in any physical experiment is rare. In Parts II and III we will largely be interested in measuring expectation values of the form $\langle a\rangle$, i.e. the coherent part of the photon field with respect to the steady state

density matrix. Such measurements are possible and have been performed via a heterodyne detection scheme [37].

The resonator output is amplified and mixed with a 'local oscillator' with frequency ω_{LO}. Assuming the system has reached its steady state so that the output field oscillates at the drive frequency μ, the resulting field is

$$\begin{aligned} & A \quad \sqrt{\kappa}\langle a\mathrm{e}^{-i\mu t} + a^{\dagger}\mathrm{e}^{i\mu t}\rangle \cos\left(\omega_{\mathrm{LO}}t + \alpha\right) && (2.27) \\ = \; & A \quad \frac{\sqrt{\kappa}}{2}\langle a\left(\mathrm{e}^{-i(\mu-\omega_{\mathrm{LO}})t+i\alpha} + \mathrm{e}^{-i(\mu+\omega_{\mathrm{LO}})t-i\alpha}\right) && (2.28) \\ & + \quad a^{\dagger}\left(\mathrm{e}^{i(\mu-\omega_{\mathrm{LO}})t-i\alpha} + \mathrm{e}^{i(\mu+\omega_{\mathrm{LO}})t+i\alpha}\right)\rangle. \end{aligned}$$

A indicates the gain. Averaging over fast frequencies $\pm(\mu + \omega_{\mathrm{LO}})$, it is now possible to extract the quadratures

$$I = \frac{1}{2}\langle a + a^{\dagger}\rangle \tag{2.29}$$

$$Q = \frac{i}{2}\langle a - a^{\dagger}\rangle \tag{2.30}$$

which correspond to the real and momentum space components of the bosonic mode. By measuring the quadratures, it is now easy to extract the expectation value of the photon operator

$$|\langle a\rangle| = \sqrt{I^2 + Q^2}. \tag{2.31}$$

Circuit QED Experiments Jaynes-Cummings physics in circuit QED and, in particular, heterodyne detection schemes have been demonstrated successfully in experiments. Bishop et al. [34] have demonstrated the dressing of dressed states in the Jaynes-Cummings model and found that it is accompanied by the supersplitting described in section 2.1. By embedding a *transmon* qubit in an on-chip cavity and tuning it into resonance, they observed that the effective two-level approximation matches experiments well at low drive strength. Additionally they saw a slight departure from this simple model as enough excitations were pumped into the cavity to make additional energy levels accessible.

The Mollow triplet in resonance fluorescence measurements, as well as photon statistics in emission from qubit-resonator systems have been studied by Lang et al. [48]. Using a qubit-resonator Jaynes-Cummings system, they generated single photons from classical resonant light. Measuring both field quadratures of the split and amplified output signal they confirmed the photon blockade effect[8] and observed sub-Poissonian photon statistics and anti-bunching. They also used this setup for measuring the resonance fluorescence spectra, which show the characteristic Mollow triplet, as well as an elastic peak at the pump frequency. The resolution of the technical challenge of measuring correlation functions in microwave systems, where linear amplifiers need to be used instead of single photon counters, was reported by Bozyigit et al. [49] where input-output theory was used to analyse field quadratures. Jaynes-Cummings systems as single photon sources have also been studied by Houck et al. [50].

Collective qubit states have been seen in [39] where three qubits were placed in a microwave resonator with one, two or three qubits at a time in resonance with the first harmonic cavity mode. As expected, the collective Rabi frequency showed the characteristic $\sqrt{N}$ scaling with the number of resonant qubits N, demonstrating that the N-qubit-cavity system behaves collectively as a single quantum system. Previously, the simple Jaynes-Cummings ladder showing a splitting between polariton states that scales as $\sqrt{n}$ for n photons inside a cavity containing a single two-level system was confirmed by Fink et al. [51].

Related work has been done by Hoffman et al. [52] who observed Rabi oscillations in qubit-cavity systems with tunable coupling strength. Hoffman et al. [53] studied the Jaynes-Cummings system in the dispersive (i.e. off-resonant) regime where the qubit effectively remains unoccupied and merely gives rise to a photon non-linearity, which then gives rise to a photon blockade effect.

As this thesis is mainly focused on larger quantum optical systems, it

[8] Only a single photon can enter the cavity at a time from the classical light. Following the emission of that photon into the resonator, the next photon can enter. This gives rise to a single photon source characterised by anti-bunched photon statistics.

should be mentioned that lattices of microwave resonators (without embedded qubits) have been studied experimentally by Underwood et al. [54].

Chapter 3

Review: The Jaynes-Cummings Hubbard Model

The primary focus of Part II is on the collective behaviour of quantum optical systems — asking the question: What happens if we couple together several cavities containing qubits, forming a lattice of quantum optical systems that interact through their photon components? Starting in 2008 [6], this question has mostly been addressed in the context of equilibrium phase transitions.

The Hamiltonian of interest is the Jaynes-Cummings Hubbard model:

$$\begin{aligned} H &= \sum_i H_i^{\mathrm{JC}} - \frac{J}{z}\sum_{\langle ij\rangle} a_i^\dagger a_j \qquad (3.1)\\ &= \sum_i \left(\omega-\mu\right) a_i^\dagger a_i + \frac{(\epsilon-\mu)}{2}\sigma_i^z + g\left(a_i\sigma_i^+ + a_i^\dagger\sigma_i^-\right) - \frac{J}{z}\sum_{\langle ij\rangle} a_i^\dagger a_j. \end{aligned}$$

The physical meaning of this model is simple: Imagine placing a two-level system inside a cavity to form a Jaynes-Cummings system. Coupling many such systems together by allowing photons to hop at rate J/z to each of the z adjacent systems, we have formed a lattice of coupled quantum optical systems. Here, we only consider the case where all sites are equivalent (no disorder) and the hopping is defined such that the total photon bandwidth is $2J$. μ acts as a chemical potential by setting the energy at which excitations can be added to the system.

3.1 Elementary Properties

We start by considering the zero temperature ground state properties, which we will summarise in a phase diagram. Assuming the resonant case $\omega = \epsilon$, we are left with the parameters $(\omega - \mu)/g$ and $J/(zg)$.

At zero hopping, $J = 0$, all lattice sites decouple and the quantum ground state is just that of the Jaynes-Cummings model with the same chemical potential on each site. The overall quantum state is the corresponding tensor product $\Pi_{\otimes i}|\mathrm{JC}\rangle_i$. Making use of the results in Chapter 2 the polariton energies are

$$E_0 = 0 \tag{3.2}$$

$$E_n^{\pm} = n(\omega - \mu) \pm g\sqrt{n} \tag{3.3}$$

and now depend on the chemical potential μ. For large negative μ, the lowest energy state is the vaccum state E_0. As μ increases, it becomes favourable to add more excitations to the system. As the upper polariton $(+)$ states are all higher in energy than the corresponding lower polariton states $(-)$, we successively move through the $n = 1, 2, 3\ldots$ lower polariton states as μ increases towards ω [44]. The overall ground state is hence $\Pi_{\otimes i}|n, -\rangle_i$ in the range $\sqrt{n-1} - \sqrt{n} \geq (\mu - \omega)/g \geq \sqrt{n} - \sqrt{n+1}$. For $\mu > \omega$, it is energetically favourable to add an infinite number of excitations, which represents an instability.

So far, this discussion involves purely Jaynes-Cummings physics as all sites are completely independent and equivalent Jaynes-Cummings systems with chemical potential μ. Considering the full lattice (still for hopping $J = 0$), each of the ground states has the same integer number of excitations. These states are known as *Mott states*. The collective physics emerges from the single site physics as the hopping rate J/z is increased: adjacent Mott states near $(\mu - \omega)/g = \sqrt{n} - \sqrt{n+1}$ hybridise to form a phase where excitations are delocalised over lattice sites. In this region, the expectation value of the photon operator is non-zero, indicating a coherent state. In analogy with other lattice models, most notably the Bose-Hubbard model

[55], this is termed *superfluid* phase. With increasing hopping rate J/z the regions of μ for which Mott states persist (i.e. are energetically favourable) shrink in size and ultimately vanish entirely. Thus there exist *Mott lobes* extending only up to a critical hopping strength that forms the tip of the lobe.

3.2 Mean-Field Theory

Many analytical and numerical studies of the equilibrium phase diagram exist: Mean-field theory [6, 44], strong-coupling theory with a random phase approximation [56], density-matrix renormalisation group calculations [57], Quantum Monte Carlo simulations [58], variational cluster calculations [59] and others. While the exact locations of the phase boundaries depend on the dimensionality and the method of calculation, all approaches find the existence and approximately correct sizes of the Mott lobes.

The simplest and most readily accessible tool for calculating the phase diagram is the mean-field approximation [6]. The difficulty in diagonalising the Jaynes-Cummings Hubbard Hamiltonian in equation (3.2) lies in the hopping term. One may approximate

$$\begin{aligned} a_i^\dagger a_j &\approx \langle a_i\rangle^* a_j + \langle a_j\rangle a_i^\dagger - \langle a_i\rangle^*\langle a_j\rangle && (3.4)\\ &= \langle a_i\rangle^* a_i + \langle a_i\rangle a_i^\dagger - |\langle a_i\rangle|^2, && (3.5)\end{aligned}$$

where the second line assumes that all sites are equivalent. As a result all lattice sites decouple. This approximation, where the photons in each cavity see the average field ('mean field') of all nearest-neighbour cavities, allows for classical correlations between lattice sites, but discards quantum correlations.

The Hamiltonian hence becomes

$$H^{\mathrm{MF}} = \sum_i \left[H_i^{\mathrm{JC}} - J\left(\langle a\rangle a_i^\dagger + \langle a\rangle^* a_i - |\langle a\rangle|^2\right)\right]. \qquad (3.6)$$

Truncating the Hilbert space at a maximum number $n_{\max}$ of excitations per site, the resulting $(2n_{\max}+1)$-by-$(2n_{\max}+1)$ matrix for any individual site

can be diagonalised numerically [6, 44]. Finding the minimum ground state energy with respect to $\langle a \rangle$ (which, due to the $U(1)$ symmetry of the Jaynes-Cummings-Hubbard Hamiltonian, can be chosen real by gauge transform), the structure of Mott lobes ($\langle a \rangle = 0$) and superfluid regions ($\langle a \rangle \neq 0$) emerges as shown in figure 3.1.

As first introduced by [44], the location of the phase boundary can be calculated analytically within perturbation theory. Treating the mean-field hopping term as a perturbation to a particular Mott state (i.e. a particular lower polariton state), one can find the second order coefficient r of the Landau expansion of the free energy,

$$F = F_0 + r|\psi|^2 + \frac{1}{2}u|\psi|^4 + \dots \tag{3.7}$$

with $\psi \equiv \langle a \rangle$. Where $r = 0$, $u > 0$, the system undergoes a second order phase transition. The Landau expansion of the ground state energy is an approximation where $|\psi| > 0$, but becomes exact on the phase boundary as $\psi \to 0$. The condition $r = 0$ translates into

$$J = \left\{ \sum_{i \in \{+,-\}} \left(\frac{|\langle n+1, i|a^\dagger|n, -\rangle|^2}{E_n^- - E_{n+1}^i + \mu} + \frac{|\langle n-1, i|a|n, -\rangle|^2}{E_n^- - E_{n-1}^i - \mu} \right) \right\}^{-1} \tag{3.8}$$

where n indicates the number of excitations and $\sum_i$ sums over all polariton states accessible from the ground state $|n, -\rangle$ by a single creation or annihilation operator.

A zero hopping ($J = 0$) picture first studied by [6] gives further insights into the structure of Mott states when the photons are detuned away from the two-level systems, $\omega \neq \epsilon$. With increasing detuning, the $n = 0$ Mott lobe grows at the expense of the others, which are shifted towards $\mu = \omega$. Zero detuning exhibits the largest $n > 0$ Mott lobes. This is shown in figure 3.1.

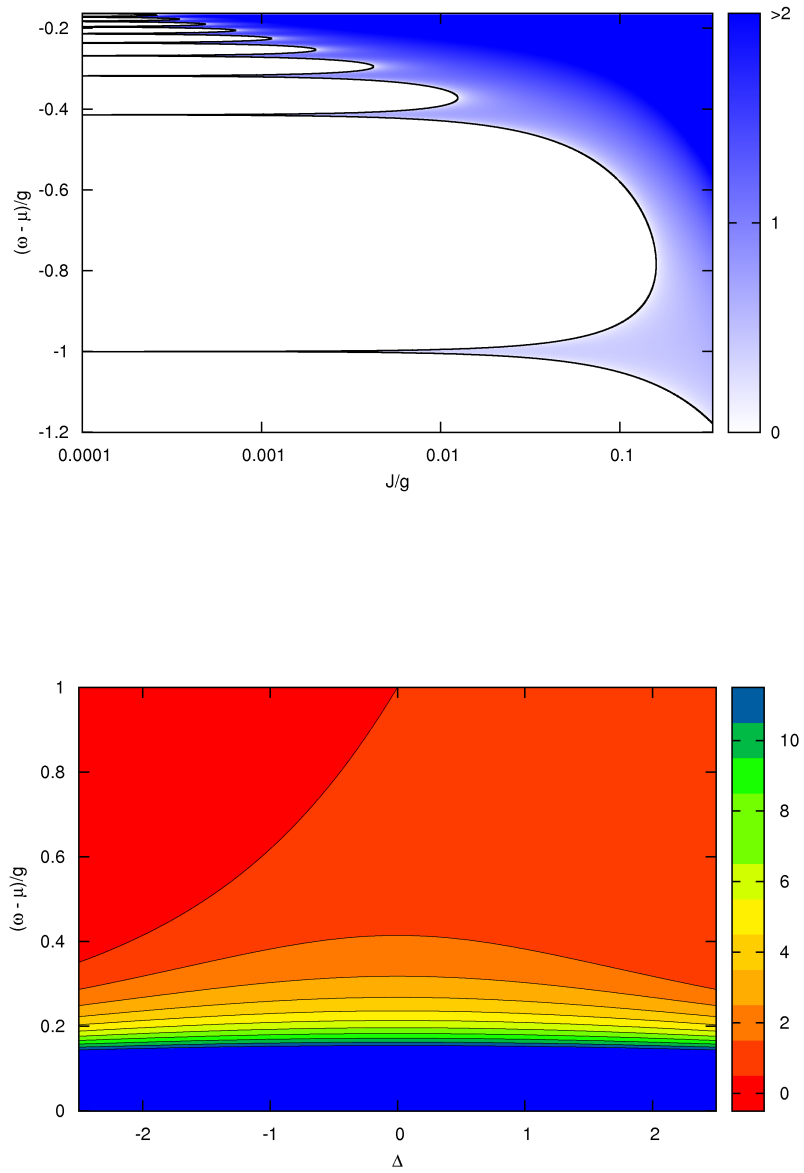

Figure 3.1: Top panel: Mean-field phase diagram of the Jaynes-Cummings Hubbard model. The Mott lobes (white) have a fixed number of excitations per site, increasing with pump frequency. The black line describes the perturbative second order phase boundary. Bottom panel: Corresponding zero hopping picture as a function of detuning. The black lines indicate the perturbative phase boundaries.

3.3 Relationship with the Bose-Hubbard Model

Attempts [6, 44] have been made to map the Jaynes-Cummings-Hubbard Model onto the Bose-Hubbard Model describing bosons b_i on a lattice with an on-site interaction $\frac{1}{2}Ub^\dagger b\left(b^\dagger b-1\right)$. However, defining an effective Hubbard-U [44],

$$U_{n\pm}=\frac{1}{n}\left(E_{n+1}^{\pm}-E_n^{\pm}+\mu\right), \tag{3.9}$$

we notice that the non-linearity is strongly dependent on the number of polaritons n per site. As a result, the Jaynes-Cummings Hubbard Model does not readily map onto the Bose-Hubbard Model.

Yet, as can be seen from the phase diagram, structural similarities do exist. Mott states at zero hopping are split by superfluid regions in both models [6, 44, 55]. Additionally, the universality class of the phase transition is the same almost everywhere[1] with the dynamical critical exponent $z=2$ [44].

[1] Using the $U(1)$ gauge symmetry, one can show that multicritical lines exist (as a function of detuning) at the tips of the Mott lobes, whereas the Bose-Hubbard model only shows multicritical points as the Jaynes-Cummings Hubbard model contains the qubit-cavity detuning as an additional parameter [44]. At these points, the universality class changes to $z=1$ in both models [56].

Part II

The Jaynes-Cummings-Hubbard Model

Chapter 4

Equlibrium Model with Inflected Spectra

In this chapter, as well as the remaining chapters of Part II, we will study the Jaynes-Cummings Hubbard model beyond the equilibrium context. Equation (3.2) describes perfect two-level systems coupled strongly to cavity modes. Experimental realisations of this model have been proposed in the context of circuit quantum electrodynamics [44], where superconducting qubits play the role of the matter degrees of freedom. While the biggest obstacle towards an experimentally feasible implementation of the Jaynes-Cummings Hubbard model is certainly the role of dissipation and the associated non-equilibrium effects (Chapters 5, 6 and 7), we will start by analysing an extension of the equlibrium model.

Using *transmon* qubits for the matter degrees of freedom inside the cavities, we realise that these are multi-level systems with an anharmonic spectrum and different transition rates between different energy levels. It is clear from the introduction that both of these facts will impact the phase diagram of this extended Jaynes-Cummings Hubbard model.

The spectrum of a transmon qubit is almost independent of the offset charge n_g, as it is designed to reduce charge noise. The transmon Schrödinger equation can be solved by Mathieu functions [45], resulting in the spectrum shown in figure 4.1. The corresponding transition matrix elements are shown

as well.

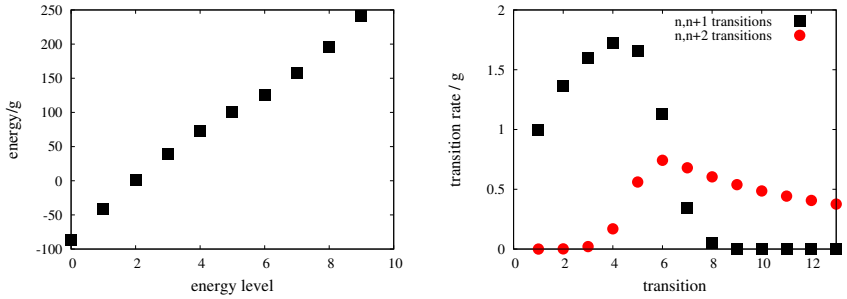

Figure 4.1: First panel: Transmon energy levels. Both positive and negative curvature are present in the spectrum. Second panel: Corresponding transition rates for transitions that are one and two excitations apart, respectively.

The low energy part of the spectrum (the effective description in terms of Cooper pairs tunnelling through the Josephson junctions is valid for energy scales below the superconducting gap) exhibits both positive and negative curvature. Depending on the offset charge, there may be finite non-number conserving transition rates (i.e. matrix elements). However, the dominant transitions are the number-conserving ones and we thus discard any other ones.

The additional energy levels and transition rates affect the mean-field phase diagram in two ways: 1. The exact eigenstates of the polaritons and thus the locations of the Mott lobes change. This is a quantitative effect that leaves the qualitative structure of the phase diagram unchanged. 2. The energy eigenstates (lower polaritons) can re-order. As a result, the Mott states no longer increase monotonically in excitation number along the vertical axis. Instead, first-order jumps between Mott states are possible, even without any superfluid phases in between. This is shown in figure 4.2.

This behaviour can be understood by analysing the zero hopping limit. In the grand canonical ensemble where the relevant energy levels are $E_n - n\mu$ for the n excitation state, the ground state may jump as a function of chemical potential μ between Mott states that differ by more than one excitation. Figure 4.3 shows the Mott lobes in the zero hopping limit as a function of detuning. Here, the lines indicate the perturbative calculation based upon

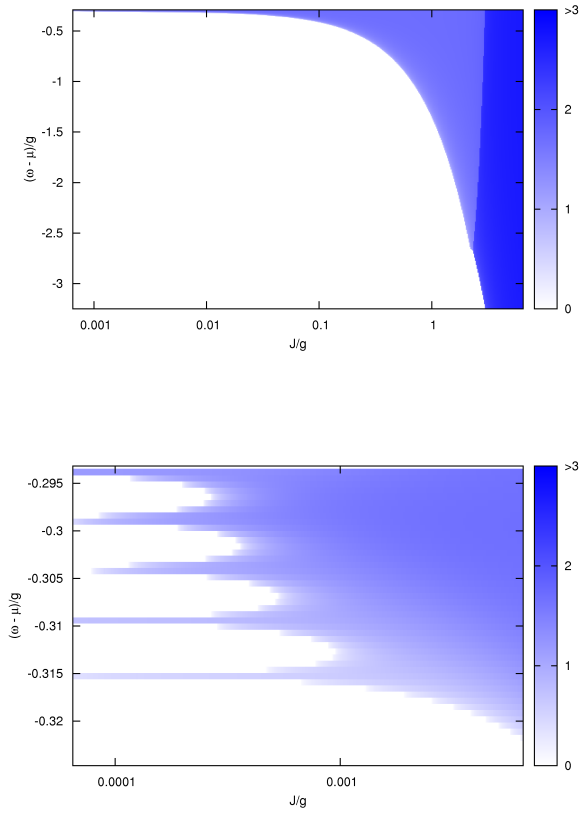

Figure 4.2: Mean-field phase diagram of the multi-level Jaynes-Cummings Hubbard model. The Mott lobes (white) have a fixed number of excitations per site, increasing with pump frequency. There is a jump due to the non-monotonicity of the energy levels measured from the chemical potential.

hybridisation. The perturbative calculation follows the same formulæ as that of the two-level case, but the summation in equation (3.8) is over all photon-transmon states accessible by a single photon creation or annihilation. Labelling the n-excitation ground state as g, the phase boundary is given by

$$J = \left\{ \sum_i \left(\frac{|\langle n+1, i|a^\dagger|n, g\rangle|^2}{E_n^g - E_{n+1}^i + \mu} + \frac{|\langle n-1, i|a|n, g\rangle|^2}{E_n^g - E_{n-1}^i - \mu} \right) \right\}^{-1} . \tag{4.1}$$

This calculation always predicts phase boundaries due to hybridisation of the n excitation state with the adjacent $(n \pm 1)$ excitation states. However, these adjacent states in excitation space are not necessarily adjacent in energy space anymore — the overall ground state is in general non-monotonic in n and is hence not restricted to $n \pm 1$ excitations. This explains the emergence of jumps between different excitations numbers.

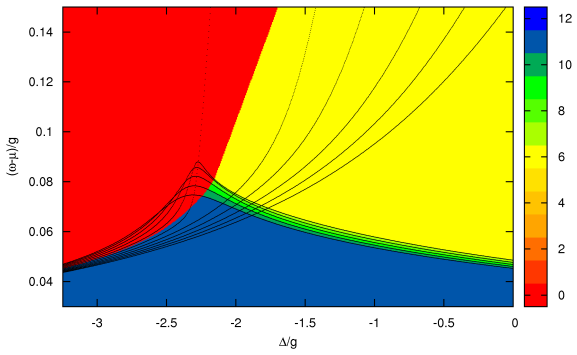

Figure 4.3: Zero hopping picture of the multi-level Jaynes-Cummings Hubbard model as a function of detuning. The black lines indicate the perturbative phase boundaries.

While this straightforward extension of the Jaynes-Cummings Hubbard model shows some non-trivial effects in the phase diagram, there are several problems with this analysis: We have somewhat arbitrarily truncated the number of transmon states considered, we have disregarded any non-number conserving interactions, we have ignored the fact that the circuit QED treatment of the transmon is only valid at energies below the superconducting gap

corresponding to only a few energy levels, and we expect the impact of drive and dissipation to be significant. As a result, while giving an idea of what the effect of additional energy levels is in an ideal system, this analysis really just serves as motivation for treating this problem more fully in its natural non-equilibrium context. In that case, studied in the remainder of Part II of this thesis, one may drive the system at or near specific transitions, which allows us to approximate the transmons as two-level systems again, ignoring higher energy levels. While we will not study the effect of additional qubit levels in the non-equilibrium context, it has been shown both numerically and experimentally [34] that they have a small but noticeable quantitative (but not qualitative) effect on the response of circuit QED systems.

Chapter 5

Non-Equilibrium Mean-Field Theory

5.1 Introduction to the JCHM with drive and dissipation

Having discussed the equilibrium mean-field theory and its extension to multi-level systems in the previous chapter, we now move on to add dissipation to the regular Jaynes-Cummings Hubbard model. Any realistic experiment on the Jaynes-Cummings Hubbard model will inevitably have to deal with the loss of photons from the cavities and the relaxation of the two-level systems. In order to compensate for the loss of excitations, we coherently pump photons into the system. The simplest pump scheme involves adding coherent photons equally to all cavities. While one may assume that this would destroy all interesting phenomena, the physics of even such a simple drive scheme turns out to be remarkably rich.

The Hamiltonian of the pumped, decaying Jaynes-Cummings Hubbard

model at pump frequency μ is

$$\begin{aligned} H &= \sum_i (\omega - \mu)\, a_i^\dagger a_i + \frac{(\epsilon - \mu)}{2}\sigma_i^z + g\left(a_i\sigma_i^+ + a_i^\dagger\sigma_i^-\right) \\ &- \frac{J}{z}\sum_{\langle ij\rangle} a_i^\dagger a_j + \sum_i f\left(a_i^\dagger + a_i\right) \end{aligned} \tag{5.1}$$

with photon and two-level system decay terms implemented in the density matrix equation of motion as

$$\frac{\mathrm{d}}{\mathrm{d}t}\rho = -i[H,\rho] + \sum_i \left(\frac{\kappa}{2}\mathcal{L}[a_i] + \frac{\gamma}{2}\mathcal{L}[\sigma_i^-]\right). \tag{5.2}$$

5.1.1 Existing Work

The body of existing work studying coupled cavity arrays out of equilibrium, and in particular the Jaynes-Cummings Hubbard model, is small. Tomadin et al. [60] have studied signatures of superfluid-Mott insulator transitions for interacting photons on a lattice by calculating the average response of an effective Bose-Hubbard model to pulsed excitation. They observed the onset of coherence with hopping in $g^{(2)}(0)$ and the photon expectation value within mean-field theory. Following the work presented below and published in [1], Grujic et al. [61] studied the related problem of emission statistics of Bose-Hubbard and Jaynes-Cummings Hubbard models. They found multi-particle features in the response of the in-cavity excitation number as a function of pump frequency. Leib and Hartmann [62, 63] have studied two coupled resonators containing qubits, mapped onto a Bose-Hubbard model. Pumping one cavity and observing the response of the other they find a transition between coherent and anti-bunched photon states as the effective non-linearity is increased, corresponding to a photon blockade effect.

5.2 Steady State Solution

After an initial transient time-evolution we expect the system to settle down to a homogeneous steady state. Like in the driven Jaynes-Cummings model

[34] as well as the equilibrium Jaynes-Cummings Hubbard model [6, 44], we characterise the steady state by the single cavity coherent photon field $\langle a_i \rangle$ and in Section 5.4 by fluctuations about the steady-state coherent photon field expressed in terms of fluorescence spectra.

5.2.1 Numerical Calculation

Time-evolving the density matrix equation of motion (5.2) for the full system of N cavities is a problem exponentially large in N, which is virtually intractable beyond two cavities. In order to be able to solve the equation of motion numerically we use the same mean-field approximation as in the equilibrium problem,

$$a_i^\dagger a_j \to \langle a_j \rangle^* a_i + \langle a_i \rangle a_j^\dagger. \tag{5.3}$$

The $|\langle a \rangle|^2$ term in equation (3.5) is proportional to the identity operator and hence does not affect the time-evolution. This turns the von Neumann equation into a single-site problem with a $|\langle a \rangle|$-dependent Hamiltonian that is self-consistently determined at every time step.

Numerically time-evolving the single site problem with the bottom of the photon band resonant with the two-level systems, $\omega - J = \epsilon$, we find the results shown in figure 5.1. At zero hopping, $J = 0$, the photon field $|\langle a \rangle|$ as a function of pump frequency shows the expected Lorentzian lineshape with an anti-resonant dip as explained by the dressing of dressed states described in Chapter 2.1. At non-zero hopping, $J > 0$, the resonance shifts along the pump frequency axis at a rate proportional to J. The anti-resonant dip, however, moves at a slower rate determined self-consistently via $|\langle a \rangle|$. As hopping increases, the anti-resonance lags so far behind the resonance that it turns into a bistability, even at relatively low hopping.

Pumping the lower polariton formed by the bottom of the photon band and the two-level system on resonance as shown in figure 5.2, we study the coherent photon field over a large range of hopping rates covering the transition from anti-bunched to coherent behaviour in figure 5.3 for different values of drive strength f. At small hopping, the coherent field again shows the expected anti-resonance: An initial increase with f as the resonance

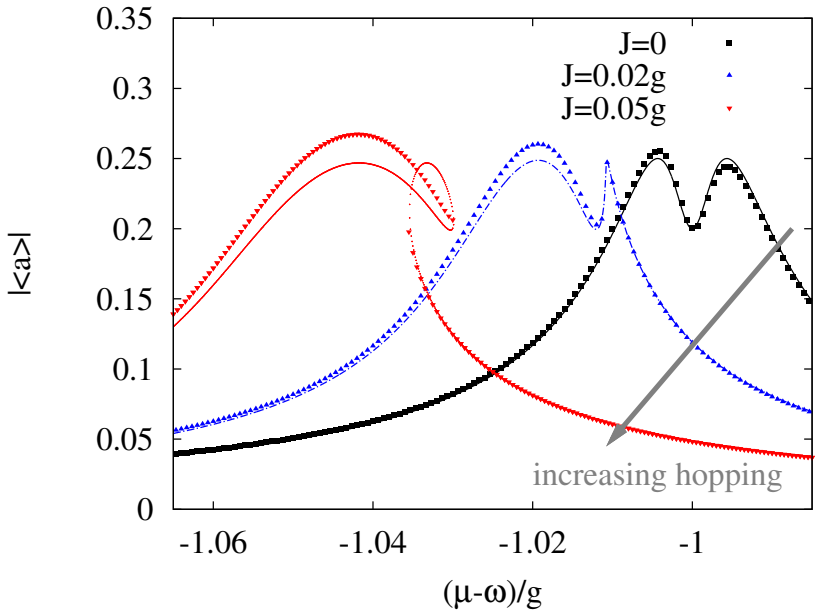

Figure 5.1: Resonant and anti-resonant features of the Jaynes-Cummings Hubbard model within mean-field theory. With increasing hopping the anti-resonant dip becomes bistable. The squares and triangles correspond to the mean-field numerical calculation, the dots and lines are the spin-chain approximation.

grows, followed by a decrease as the anti-resonant saturation effect takes over. This gives rise to an unusual non-monotonic ordering of the cavity photon response with drive strength. At large hopping $J \gg g$ the coherent field increases monotonically with drive strength f with a smooth crossover in between those two regimes.

Further insight can be gained from the coherence function $g^{(2)}(t = 0)$, which is shown in figure 5.4. At small hopping, $g^{(2)}$ is close to zero indicating a quantum mechanical state. This agrees with the anti-resonant behaviour corresponding to an effective two-level system. At large hopping, $g^{(2)}$ approaches one, which corresponds to the photons being in a coherent state.

The additional lines in figure 5.3 at small and large hopping correspond to effective models that can be solved analytically. In the quantum regime (small J) a spin-chain model of on-site effective two-level systems coupled by an effective hopping term approximates the Jaynes-Cummings Hubbard

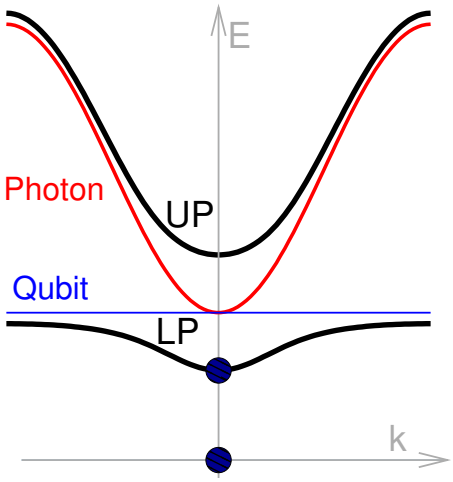

Figure 5.2: Schematic of the energy levels in the Jaynes-Cummings Hubbard model. The photons form a band, the lowest state of which is resonant with the in-cavity two-level system. The pump frequency is near the transition of the vacuum state and the bottom of the lower polariton band.

model well. Where $J \gg g$, the photon coherent state warrants a semiclassical treatment. Both are discussed in the following sections.

5.2.2 Small Hopping: A Spin-Chain Model

At small hopping rate $J \ll g$, excitations are not significantly delocalised across the lattice. At small drive strength, the occupation per cavity is significantly less than 1. We may therefore treat the Jaynes-Cummings Hubbard model as a set of on-site polaritons coupled to polaritons on adjacent sites via J. Due to the low occupation, only the lowest eigenstates need to be considered.

The in-cavity effective two-level system formed by the vacuum state and the lower polariton — which is the transition near which we are driving the system — can be described in terms of Pauli matrices $\{\tau\}$ using the Hamiltonian

$$H_{\mathrm{TLS}} = -\frac{\tilde{J}}{z}\sum_{\langle ij\rangle}\tau_i^+\tau_j^- + \frac{\tilde{\Delta}}{2}\sum_i \tau_i^z + \tilde{f}\sum_i\left(\tau_i^+ + \tau_i^-\right). \tag{5.4}$$

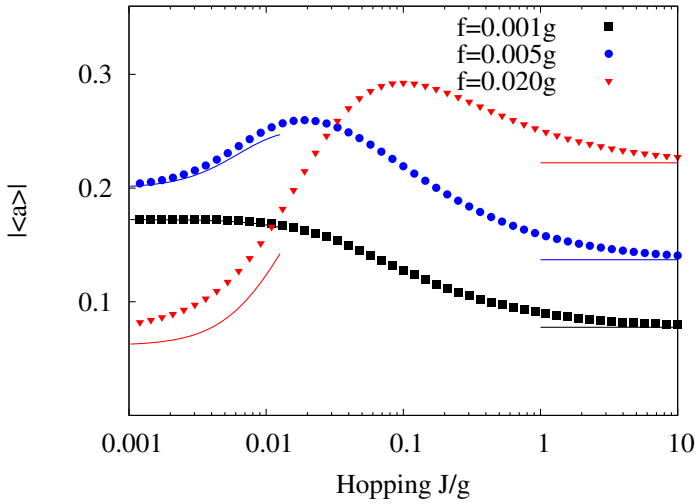

Figure 5.3: Expectation value of the photon operator as a function of hopping rate, keeping the two-level system resonant with the bottom of the photon band and pumping the lower polariton as described in figure 5.2. The pump strength increases from black to blue to red, corresponding to the anti-resonant behaviour. At large hopping the cavity response increases with drive as expected when the photons are in a coherent state delocalised over the entire lattice. The lines at small hopping correspond to the spin-chain model, at large hopping the asymptotes are given by semiclassics.

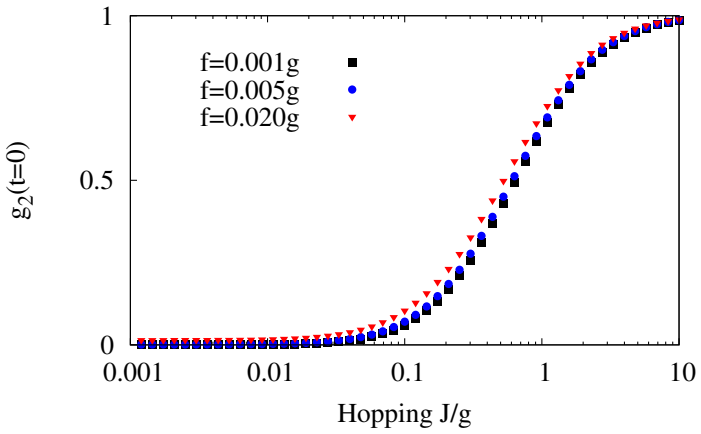

Figure 5.4: Behaviour of the photon correlation function $g^{(2)}$ corresponding to the range of hopping shown in figure 5.3. At small hopping the behaviour is quantum mechanical. As hopping increases the photons become coherent, justifying the semiclassical approximation.

Using $\tilde{\omega} = \omega - \mu$ and $\tilde{\epsilon} = \epsilon - \mu$ with $2\theta = \tan^{-1}(2g/(\tilde{\omega} - \tilde{\epsilon}))$ to denote the polariton angle, we define the effective two-level system energy as $\tilde{\Delta} = \left(\tilde{\omega} + \tilde{\epsilon} - \sqrt{(\tilde{\omega} - \tilde{\epsilon})^2 + 4g^2}\right)/2$, the effective hopping rate $\tilde{J} = J \sin^2\theta$ and the effective pump strength $\tilde{f} = -f \sin\theta$. The decay rates are amalgamated into a single two-level system decay rate $\tilde{\kappa} = \kappa \sin^2\theta + \gamma \cos^2\theta$.

Using the mean-field decoupling again to turn the above problem into a single site problem we can find the steady state of the equation of motion

$$\dot{\rho} = -i[H_{\mathrm{TLS}}, \rho] + \frac{\tilde{\kappa}}{2}\mathcal{L}[\tau^-] = 0 \tag{5.5}$$

by parameterising the density matrix as

$$\rho = \frac{1}{2}\begin{pmatrix} 1+z & 2\phi \\ 2\phi^* & 1-z \end{pmatrix}. \tag{5.6}$$

The steady state equations are

$$0 = \partial_t z = -2i\tilde{f}\left(\phi^* - \phi\right) - \tilde{\kappa}\left(1 + z\right) \tag{5.7}$$

$$0 = 2\partial_t \phi = -2i\Delta\phi + 2iz\left(\tilde{f} - \tilde{J}\phi\right) - \tilde{\kappa}\phi \tag{5.8}$$

which lead to a third order polynomial in z, giving rise to either a single stable solution or three solutions, two of which are stable. The corresponding values of the coherent photon field are shown in figure 5.1 as solid lines and confirm both the anti-resonant and bistable behaviour found numerically. The anti-resonant behaviour is also evident from figure 5.3 with the discrepancy between the numerics and the spin-chain model growing with drive strength f. This is due to the fact that pumping more excitations into the system requires more than the lowest two excitations per cavity to capture the physics accurately, leading to the (slow) breakdown of the spin-chain model.

Equations (5.7) and (5.8) also show the effect of the mean-field decoupling. The pump term in the basis of the two-level system, $\tilde{f}$, has been modified by an effective pump $-\tilde{J}\phi$ induced by the mean photon field on adjacent sites.

Equations (5.7) and (5.8) can be re-written as

$$\phi = \frac{\tilde{f}\left(\tilde{\Delta} + \tilde{J}z - i\tilde{\kappa}/2\right)}{\left(\tilde{\Delta} + \tilde{J}z\right)^2 + \frac{\tilde{\kappa}}{2} + 2\tilde{f}^2} \tag{5.9}$$

$$\frac{1+z}{2} = \frac{\tilde{f}}{\left(\tilde{\Delta} + \tilde{J}z\right)^2 + \frac{\tilde{\kappa}}{2} + 2\tilde{f}^2} \tag{5.10}$$

with $\langle\tau^-\rangle = \phi$ and $\langle\tau^z\rangle = z$. Defining an effective detuning $\delta = \tilde{\Delta} + \tilde{J}z$, the onset of bistability is given by the value of $\tilde{J}$ at which multiple solutions for z and ϕ exist. As described in [2], this may be found as $\mathrm{d}\tilde{\Delta}/\mathrm{d}\delta = 0 = \mathrm{d}^2\tilde{\Delta}/\mathrm{d}\delta^2$,

giving a critical value of re-scaled hopping

$$\tilde{J}_c = \frac{4}{\tilde{f}^2}\left(\frac{2\tilde{f}^2 + \left(\frac{\tilde{\kappa}}{2}\right)^2}{3}\right)^{\frac{3}{2}}. \tag{5.11}$$

5.2.3 Large Hopping: A Semi-Classical Model

The other limiting case of the Jaynes-Cummings Hubbard model is the large hopping regime $J \gg g$. As discussed above, the applicability of a semi-classical model in this regime is justified by our intuitive understanding of photon delocalisation as well as the mean-field numerics. In the Heisenberg equations of motion for the two-level system and photon operators we can replace all photon operators by c-numbers describing coherent states.[1] The corresponding steady state equations of motion become

$$\begin{aligned} -i(\omega - J)\phi - if - igp - \frac{\kappa}{2}\phi &= 0 & (5.12)\\ -i(\omega - J)p + 2igs^z\phi - \frac{\gamma}{2}p &= 0 & (5.13)\\ -ig(\phi p^* - \phi^* p) - \gamma\left(s^z + \frac{1}{2}\right) &= 0. & (5.14) \end{aligned}$$

Here, $p = \langle\sigma^-\rangle$, $s^z = \langle\sigma^z\rangle$, $\phi = \langle a\rangle$. The resulting asymptotic values, which are independent of hopping when the two-level systems are kept resonant with the bottom of the photon band, are

$$\begin{aligned} p &= \frac{2igs^z}{i(\omega - J) + \gamma/2}\phi & (5.15)\\ \phi &= \frac{if}{-i(\omega - J) + \frac{2g^2 p}{i(\omega - J) + \gamma/2} - \kappa/2}. & (5.16) \end{aligned}$$

Substituting these values into the third of the steady state Heisenberg equations we find a cubic in s^z with one physical (real) and two unphysical (complex) solutions. These can then be used to calculate the coherent photon

[1] This is equivalent to using the Jaynes-Cummings Hubbard Hamiltonian with only the $k = 0$ photon mode, although we will be considering localised photons later for the fluorescence spectra.

field ϕ. As shown in figure 5.3, these values form perfect asymptotes in the plot of $|\langle a \rangle|$ as a function of J.

5.2.4 'Phase diagram' out of equilibrium

Analysing the mean-field steady state coherent photon field as a function of both hopping and pump frequency while keeping the two-level systems resonant with the bottom of the photon band, we can plot the single cavity response in analogy with the mean-field phase diagram, as shown in figure 5.5. The diagram shows the resonant and anti-resonant behaviour, as well as a faint line where the pump frequency is resonant with the transition between the two photon state and the vacuum. This line becomes more pronounced as the drive strength is increased. Cuts across this phase diagram further illustrate how the initially ($J = 0$) symmetric response of the system becomes asymmetric with increasing hopping.

5.3 A note about mean-field theories and semi-classics

Within time-evolving block decimation discussed in the Introduction and Chapter 7, the extreme case of bond dimension $\chi = 1$ can be interpreted as retaining purely classical (i.e. c-number) correlations between sites. This corresponds to a 'mean-field' theory. The traditional way of imposing mean-field approximations is by replacing an operator quantity on sites adjacent to the one under consideration (e.g. a photon annihilation operator a) by their expectation values. Effectively, the system on the site under consideration feels a classical average ('mean-field') of the quantum operators on neighbouring sites.

This is distinct from the semi-classical approximation, which we employ in Section 5.2.3 as well. Semi-classics also involves replacing quantum operators by c-numbers, however, in this case the field *inside* the cavity under consideration is approximated as classical, rather than approximating the effect of adjacent cavities as classical.

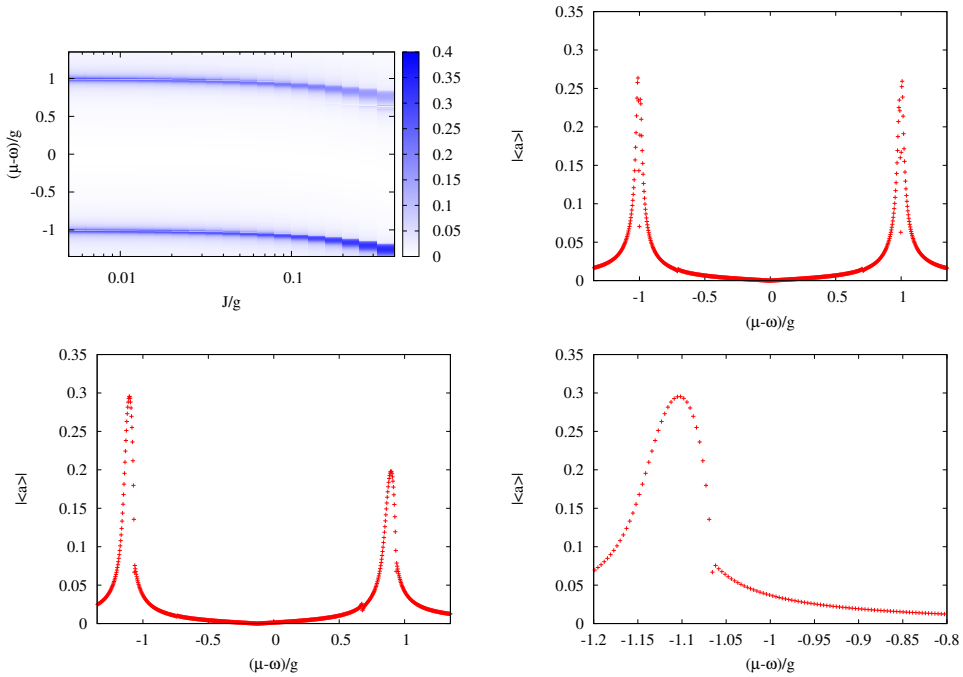

Figure 5.5: Coherent photon field of the Jaynes-Cummings Hubbard model out of equilibrium. Top-left panel: Non-equilibrium version of figure 3.1. Top-right panel: Response at small hopping ($J = 0.004g$). Bottom panels: Response at larger hopping ($J = 0.126g$), illustrating the asymmetry at non-zero hopping.

Mean-field theory does not necessarily imply homogeneity across the entire lattice. However, in the disorder-free case the simplest approximation scheme is homogeneous and can be implemented by using the on-site expectation value of quantum operators to represent the average fields from adjacent sites. This is the scheme used in Chapter 5. A relaxation of this scheme is discussed in [2], where energy disorder between sites is implemented within stochastic mean-field theory. In this case, the correlations between sites are still classical in the mean-field sense, but the system is no longer homogeneous.[2] Homogeneity is also lost when calculating two-time correlation functions (e.g. for the fluorescence spectra), as the disturbance of the system at the earlier time will propagate across the system inhomogeneously until the correlation function is calculated at the later time.

5.4 Fluctuations about the Steady State: Fluorescence Spectra

5.4.1 Idea

Having discussed the steady state coherent photon field $|\langle a\rangle|$ in detail, we may analyse the response of the steady state to the addition or removal of a photon. By the Wiener-Khintchine theorem [40, 41], we can Fourier transform the response function $\langle a_i(t)a_i^\dagger(0)\rangle$ in order to obtain the fluorescence spectrum

$$\mathcal{S}(\omega) = 2\,\Re\int_0^\infty \mathrm{d}t \mathrm{e}^{i\omega t}\langle a_i^\dagger(t)a_i(0)\rangle_{\text{steady state}}. \tag{5.17}$$

Using the quantum regression theorem, this may be calculated as

$$S(\omega) = 2\,\Re\int_0^\infty \mathrm{d}t \mathrm{e}^{i\omega t}\langle a_i^\dagger(t)\rangle_{\rho'} \tag{5.18}$$

[2] In the case of stochastic mean-field theory, this is implemented by drawing realisations of disorder from appropriate distribution functions.

with the initial condition $\rho' = a_i(0)\rho_{\text{steady state}}$.

a_i and $a_i^\dagger$ refer to photons in the same single cavity. This means that we are calculating the single cavity fluctuations (rather than those in the photon band or any other photon mode).

5.4.2 Numerical Calculation

Having calculated the mean-field steady state of the density matrix by simple time-evolution as described in Chapter 5.2.1, we apply the photon annihilation operator, time-evolve and calculate $\langle a^\dagger \rangle$ at every time step. The Fourier transform (5.18) then gives rise to the spectrum shown in Figure 5.6.

The left-hand panel shows the low energy fluorescence spectrum as a function of hopping for small drive strength f. At small hopping there are fluorescence peaks at $\pm 2g$, corresponding to the upper polariton. The effective two-level system formed by the lower polariton and the vacuum state forms a Mollow triplet split by $\sim \sqrt{2}gf$. This is not resolved in the figure due to the small value of f.

As hopping increases, the upper polaritons move to higher energies. The Mollow triplet splits up to an asymptotic value of $\omega = \pm g$ as $J \to \infty$. This asymptotic behaviour can be viewed as off-resonance fluorescence. While the relevant photons for the asymptotic $J \to \infty$ behaviour of the steady state are those of the $k = 0$ (bottom of the photon band) state, the fluctuations in a single cavity are fluctuations in the cavity mode. As the bottom of the photon mode is kept resonant with the two-level systems ($\omega - J = \epsilon$), the cavity photons (at frequency ω) are far from resonance with the two-level systems. The pump, however, is a frequency g away from the two-level systems, such that the two-level systems are pumped off resonance, which leads to the fluorescence peaks at frequencies $\pm g$.

The right-hand panel of figure 5.6 shows the spectra for large hopping $J = 10g$ as the drive strength is increased. This drives the fluorescence peaks further apart.

There is a technicality involved in calculating the fluorescence spectrum. As the initial annihilation operator is applied, the disturbance travels across

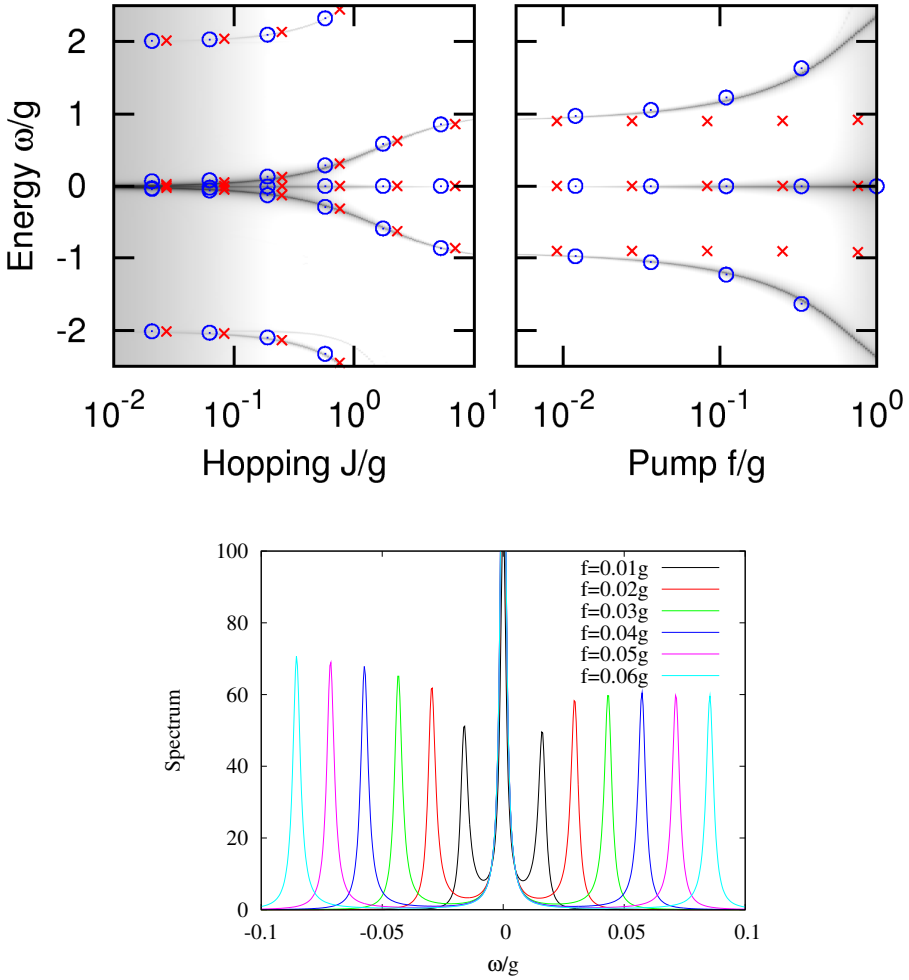

Figure 5.6: Fluorescence spectra of the mean-field Jaynes-Cummings Hubbard model. Top panel: The Mollow triplet at small hopping (which is not resolved in this figure) broadens as the hopping rate increases. This effect can be thought of as off-resonant fluorescence as the photon and two-level system energies diverge with $J \to \infty$ because we are considering fluctuations in a single cavity rather than the photon band. The right-hand panel shows that the triplet is further broadened by increasing drive strength. The blue circles correspond to the semiclassical calculation. They match well except at very small hopping (not visible on this scale). The red crosses are derived from the spin-chain model which is valid whenever the occupation is small. Discrepancies are only significant when a large drive strength increases the occupation. Bottom panel: Small hopping ($J = 0.005g$) spectra showing how the Mollow triplet splits as drive strength increases.

the lattice as the adjacent cavities see an altered photon field. As the number of nearest-neighbours z increases, this effect disappears as $1/z$. In order to study this effect in more detail, we set up a lattice where each site is time-evolved within the mean-field approximation. As shown in figure 5.7 for small coordination numbers z the spectrum has negative portions. This shows that the quantum regression theorem is strictly speaking not applicable.[3] However, as z increases this effect vanishes: The effect on the sites adjacent to the one whose fluctuations we are studying scales as $1/z$. The back-action on the cavity under consideration therefore scales as $z \times \frac{1}{z} \times \frac{1}{z} = \frac{1}{z}$.

The lattices used to demonstrate this effect are one-dimensional and two-dimensional square lattices, as well as a Bethe lattice that branches out in such a way that the coordination number can be adjusted arbitrarily. The spectra shown in figure 5.6 refer to the large z limit where mean-field theory as well as the quantum regression theorem are applicable.

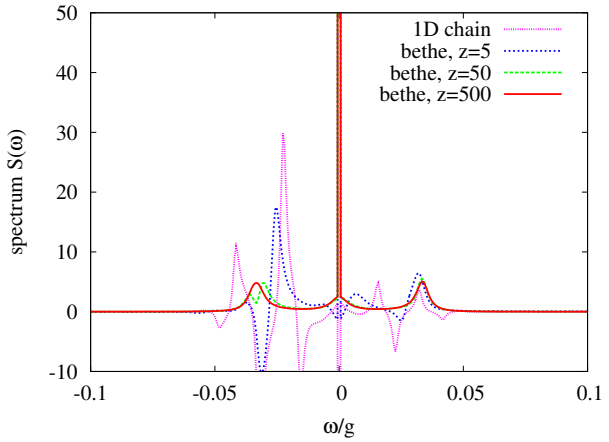

Figure 5.7: Convergence of fluorescence spectra with increasing coordination number. While the one-dimensional mean-field chain exhibits spectra with significant negative (unphysical) parts, the negative portions disappear as the coordination number is increased as shown using a Bethe lattice.

[3]The applicability requires a reservoir that is unchanged by the system operators, as well as a unitary time evolution [11].

5.4.3 The Spin-Chain Model

In addition to the numerical calculation, one may extract the locations of the fluorescence peaks from the spin-chain model. As the mean-field decoupled spin-chain model describes a single two-level system (with parameters that depend on the mean field steady state), the calculation for the Mollow triplet applies [42].

Applying the Laplace transformation $\mathscr{L}[f(t)](s) = \int_0^\infty \mathrm{d}t\, f(t)e^{-st}$, which allows us to directly impose the initial condition $\tau^-\rho$, the equation of motion for fluctuations about the steady state is

$$s\rho = -i\left[H_{\mathrm{MFSS}}, \rho\right] + \tau^-\rho_{\text{steady state}}. \tag{5.19}$$

MFSS refers to the Hamiltonian in the restricted Hilbert space that is formed by the mean-field decoupling, and whose parameters are fixed at the steady state values. This equation can be re-written in terms of a vector

$$\rho^{\#} = \begin{pmatrix} \frac{1+z}{2} & \phi & \phi^* & \frac{1-z}{2} \end{pmatrix}^T \tag{5.20}$$

as

$$\begin{aligned} s\rho^{\#} &= M\rho^{\#} + \left[\tau^-\right]^{\#}\rho^{\#}_{\text{steady state}} \qquad (5.21)\\ M &= \begin{pmatrix} -\tilde{\kappa} & i(\tilde{f}-\tilde{J}\phi^*) & -i(\tilde{f}-\tilde{J}\phi) & 0 \\ i(\tilde{f}-\tilde{J}\phi) & -i\Delta-\frac{\tilde{\kappa}}{2} & 0 & -i(\tilde{f}-\tilde{J}\phi) \\ -i(\tilde{f}-\tilde{J}\phi^*) & 0 & i\Delta-\frac{\tilde{\kappa}}{2} & i(\tilde{f}-\tilde{J}\phi^*) \\ \tilde{\kappa} & i(\tilde{f}-\tilde{J}\phi^*) & -i(\tilde{f}-\tilde{J}\phi) & 0 \end{pmatrix} \\ \left[\tau^-\right]^{\#}\rho^{\#}_{\text{steady state}} &= \begin{pmatrix} 0 & 0 & \frac{1+z}{2} & \phi \end{pmatrix}^T. \end{aligned}$$

The fluorescence spectrum can be found by substituting $s \to s_\nu = -i\nu + 0^+$ as

$$\mathcal{S}(\nu) = 2\Re\left[\begin{pmatrix} 0 & 0 & 1 & 0 \end{pmatrix}(M - s_\nu I)^{-1}\begin{pmatrix} 0 \\ 0 \\ \frac{1+z}{2} \\ \phi \end{pmatrix}\right]. \tag{5.22}$$

The locations of these peaks are shown in figure 5.6 as red crosses. They confirm the validity of the spin-chain model: When the drive strength is small enough that the relevant physics may be captured by a two-dimensional Hilbert space, the spin-chain model confirms the numerical results. However, as more excitations are added to the system, a single two-level system per site is no longer sufficient and a more complete description becomes necessary.

In order to calculate the emission from the upper polaritons, the same calculation may be repeated for the effective two-level system formed by the upper polariton and the vacuum state. The corresponding results are also shown in figure 5.6.

5.4.4 The Semi-Classical Model

In order to calculate the locations of the fluorescence peaks within the semi-classical model, we expand about the steady state coherent field $\phi \to \phi + \delta\phi$, the spin lowering operator $p \to p + \delta p$ and the z-spin component $s^z \to s^z + \delta s^z$ with $\delta\phi = \alpha e^{-i\eta t} + \beta^* e^{i\eta^* t}$, $\delta p = ce^{-i\eta t} + d^* e^{i\eta^* t}$ and $\delta s_z = he^{-i\eta t} + h^* e^{i\eta^* t}$.[4] In the basis of (a, b^*, c, d^*, h) the locations of the emission peaks are given by the eigenvalues of the matrix

$$\begin{pmatrix} \delta_r - i\frac{\kappa}{2} & 0 & g & 0 & 0 \\ 0 & -\delta_r - i\frac{\kappa}{2} & 0 & -g & 0 \\ -2gs_z & 0 & \delta_q - i\frac{\gamma}{2} & 0 & -2g\phi \\ 0 & 2gs_z & 0 & -\delta_q - i\frac{\gamma}{2} & 2g\phi^* \\ gp^* & -gp & -g\phi^* & g\phi & -i\gamma \end{pmatrix}. \tag{5.23}$$

$\delta_r = (\omega - \mu) - J$ and $\delta_q = \epsilon - \mu$. The resulting spectra are shown in figure 5.6 as blue circles. At small hopping and low drive strength (the left-hand edge of the left-hand panel) there is a mismatch between the semi-classical model and the numerics. This is because the semi-classical approximation requires a coherent photon state, which is not present in the strongly quantum mechanical regime of $J \ll g$. In all other regimes, there is an accurate match

[4] The annihilation and spin lowering operators can take complex expectation values, whereas the z-spin component is always real.

with the numerics.

Chapter 6

Keldysh Path Integral Formulation

Taking the Jaynes-Cummings Hubbard model beyond the mean-field treatment presented in the previous chapter, there are two limits that are intuitively easy to understand: When the hopping J between cavities is large, the photons delocalise over the lattice, giving rise to a coherent photon state coupled to the two-level systems. In contrast, for small hopping J we expect a mostly quantum mechanical treatment of strong on-site photon blockade with weak entanglement between sites to apply. While the latter justifies the use of time-evolving block decimation (see next chapter), the former suggests the applicability of a Keldysh path integral formulation where a saddle point approximation yields a spatially homogeneous ($k = 0$) state with Green functions describing second-order fluctuations about the mean-field state.

The approach of finding a saddle point solution and fluctuations has been applied previously in quantum optics to the related problem of out-of-equilibrium polariton condensation [16]. In this chapter we apply the same approach to the Jaynes-Cummings Hubbard model with dissipation and coherent drive on all sites.[1]

[1]The homogeneous coherent drive determines the phase of the saddle point solution. This is distinct from the calculation in [16] in that we do not need to account for phase fluctuations at all orders, whereas the phase symmetry in the polariton condensation problem is not broken externally making phase fluctuations relevant at all orders.

6.1 Saddle point equation

In this chapter we use a slightly different model to describe the same physical system of qubits in a cavity array: We represent the two-level systems as two fermionic degrees of freedom a and b with the constraint $b_i^\dagger b_i + a_i^\dagger a_i = 1$, such that $a^\dagger b$ and $b^\dagger a$ are lowering and raising operators for the two-level systems. The two-level systems decay by coupling each of the fermionic degrees of freedom to a separate set of freely evolving bath modes which can be integrated out. As these differences may have a significant effect on the physics, any quantitative comparison of this model with the Jaynes-Cummings Hubbard model as described in the previous chapters is difficult.

Altering our notation (in line with [16]), we start with the system Hamiltonian

$$\begin{aligned} H &= \sum_i \epsilon \left(b_i^\dagger b_i - a_i^\dagger a_i \right) + \sum_i \omega_c \psi_i^\dagger \psi_i + \sum_i \frac{g}{\sqrt{N}} \left(a_i^\dagger b_i \psi_i^\dagger + \text{h.c.} \right) \quad (6.1) \\ &- t \sum_{\langle ij \rangle} \left(\psi_i^\dagger \psi_j + \text{h.c.} \right) - \mu \hat{N} + \sum_i f \left(\psi_i^\dagger + \psi_i \right). \quad (6.2) \end{aligned}$$

Throughout this chapter, the bosonic operators ψ_i describe photons on site i, $t = J/z$ describes the hopping and the two-level systems are described by two fermionic operators a_i and b_i per site. The operator counting the total number of excitations in the system is $\hat{N} = \sum_i \left(b_i^\dagger b_i - a_i^\dagger a_i + \psi_i^\dagger \psi_i \right)$ and the Hamiltonian has been transformed to the frame rotating at the pump frequency μ.

The reason for using two fermionic degrees of freedom to describe the two-level systems is the possibility of integrating out these degrees of freedom in order to arrive at a path integral in terms of a (rather complicated) action involving only the bosonic field. The condition $b_i^\dagger b_i + a_i^\dagger a_i = 1$ will be enforced on average by choosing appropriate occupation functions.

Absorbing the pump frequency μ into the photon and two-level system energies ($\tilde{\epsilon}$ and $\tilde{\omega}_c$), representing the photon operators in Fourier space with $\omega_k = \omega_c - zt \cos k$ and using freely-evolving bosonic and fermionic baths, we

have the action terms

$$
\begin{aligned}
S_{\text{total}} &= S_{\text{system}} + S_{\text{baths}} && (6.3)\\
S_{\text{system}} &= \sum_k \bar{\psi}_k \left(i\partial_t - \tilde{\omega}_k\right) \psi_k && (6.4)\\
&+ \sum_{i,k} \bar{\phi}_i \left(i\partial_t - \epsilon_i \sigma^z - g(\bar{\psi}_k e^{ik\cdot r_i}\sigma^- + \psi_k e^{-ik\cdot r_i}\sigma^+)\right) \phi_i \\
S_{\text{baths}} &= \sum_p \bar{\Psi}_p \left(i\partial_t - \omega_p^{\psi}\right) \Psi_p + \sum_i \bar{\Phi}_j \left(i\partial_t - \omega_j^{\phi}\right) \Phi_j \\
&- \sum_{ij} \left(g_{ij}^A(\bar{A}_j a_i + A_j \bar{a}_i) + g_{ij}^B(\bar{B}_j b_i + B_j \bar{b}_i)\right) \\
&- \sum_{pk} g_{pk}^{\psi}(\bar{\Psi}_p \psi_k + \Psi_p \bar{\psi}_k)
\end{aligned}
$$

where $\phi_i = \begin{pmatrix} b_i & a_i \end{pmatrix}$ describes the fermions and the Pauli matrices σ act on the (b, a) space. By stipulating that reservoirs be unaffected by system operators and integrating over bath modes, the reservoir operators can be turned into effective decay rates [16].

By transforming to classical and quantum operators on the closed time contour as described in the introduction and using the sum over Fourier modes $\lambda_{\text{q,cl}} = \frac{1}{\sqrt{N}} \sum_k \psi_{\text{q,cl}}(k) e^{-ik\cdot r_i}$ the action can be written as

$$
\begin{aligned}
S &= \sum_k \begin{pmatrix} \bar{\psi}_{\text{cl}}(k) & \bar{\psi}_{\text{q}}(k) \end{pmatrix} D^{-1} \begin{pmatrix} \psi_{\text{cl}}(k) \\ \psi_{\text{q}}(k) \end{pmatrix} && (6.5)\\
&+ \sum_i \begin{pmatrix} \bar{b}_{\text{cl}} & \bar{a}_{\text{cl}} & \bar{b}_{\text{q}} & \bar{a}_{\text{q}} \end{pmatrix} G^{-1} \begin{pmatrix} b_{\text{cl}} \\ a_{\text{cl}} \\ b_{\text{q}} \\ a_{\text{q}} \end{pmatrix} && (6.6)\\
&- \sqrt{2} f \left(\bar{\psi}_{\text{q}}(0) + \psi_{\text{q}}(0)\right) && (6.7)
\end{aligned}
$$

where

$$G^{-1} = \begin{pmatrix} 0 & -\frac{g}{\sqrt{2}}\lambda_{\mathrm{q}} & i\partial_t - \tilde{\epsilon} - i\gamma & -\frac{g}{\sqrt{2}}\lambda_{\mathrm{cl}} \\ -\frac{g}{\sqrt{2}}\bar{\lambda}_{\mathrm{q}} & 0 & -\frac{g}{\sqrt{2}}\bar{\lambda}_{\mathrm{cl}} & i\partial_t + \tilde{\epsilon} - i\gamma \\ i\partial_t - \tilde{\epsilon} + i\gamma & -\frac{g}{\sqrt{2}}\lambda_{\mathrm{cl}} & 2i\gamma F_B & -\frac{g}{\sqrt{2}}\lambda_{\mathrm{q}} \\ -\frac{g}{\sqrt{2}}\bar{\lambda}_{\mathrm{cl}} & i\partial_t + \tilde{\epsilon} + i\gamma & -\frac{g}{\sqrt{2}}\bar{\lambda}_{\mathrm{q}} & 2i\gamma F_A \end{pmatrix} \tag{6.8}$$

is the inverse fermionic Green function and

$$D^{-1} = \begin{pmatrix} 0 & i\partial_t - \tilde{\omega}_k - i\kappa \\ i\partial_t - \tilde{\omega}_k + i\kappa & 2i\kappa \end{pmatrix} \tag{6.9}$$

is the inverse photon Green function. κ and γ are the photon and two-level system decay rates, respectively, and $F_A = -1$ and $F_B = 1$ describe the occupation of the decay baths corresponding to the fermionic degrees of freedom (assuming the two-level systems to decay into an empty bath).

In the path integral

$$Z \propto \int \prod \mathcal{D}\left(\bar{\psi}_i, \psi_i\right) \prod \mathcal{D}\left(\bar{a}_i, a_i, \bar{b}_i, b_i\right) \, \mathrm{e}^{i \int_C \mathrm{d}t \, S} \tag{6.10}$$

the action is now quadratic in the as and bs and one can hence integrate over the fermionic degrees of freedom in order to obtain the effective action

$$S = S_0 - i\mathrm{tr} \, \log G^{-1}. \tag{6.11}$$

The corresponding saddle point $\frac{\partial S}{\partial \bar{\psi}_{\mathrm{q}}(0)} = 0$ for the $k = 0$ classical field is

$$\left(-\tilde{\omega}_0 + i\kappa\right) \psi_{\mathrm{cl}}(0) - \sqrt{2} f = i\mathrm{tr} \left(G \frac{\partial G^{-1}}{\partial \bar{\psi}_{\mathrm{q}}(0)} \right) \tag{6.12}$$

with

$$\frac{\partial G^{-1}}{\partial \bar{\psi}_{\mathrm{q}}(0)} = -\frac{g}{\sqrt{2N}} \sigma^- \sigma^0_K. \tag{6.13}$$

Here we use Pauli matrices with subscript K acting on Keldysh $(\mathrm{cl}, \mathrm{q})$ space.

Defining $E = \sqrt{\tilde{\epsilon}^2 + g^2|\psi_\mathrm{f}|^2}$, the trace term becomes[2]

$$G^K_{ba}(\nu) = -4i\gamma \frac{g}{\sqrt{N}} \psi_\mathrm{f} \frac{\tilde{\epsilon} + i\gamma}{((\nu - i\gamma)^2 - E^2))\,((\nu + i\gamma)^2 - E^2))}. \tag{6.14}$$

Here we are using the forward field ψ_f which corresponds to the physical field in the cavity. Integrating over frequencies ν by the residue theorem of complex analysis we find

$$(-\tilde{\omega}_0 + i\kappa)\,\psi_\mathrm{f} - f = -g^2 \psi_\mathrm{f} \frac{\tilde{\epsilon} + i\gamma}{2\,(E^2 + \gamma^2)}. \tag{6.15}$$

This is the mean-field equation. Due to the presence of the coherent pump term there is no $\psi_\mathrm{f} = 0$ solution. The pump not only defines a non-zero coherent field amplitude, but also sets the phase of the photon field. As a result, we need to take into account anomalous as well as normal self-energies when calculating the luminescence spectrum using second order fluctuations. However, there is no need to consider phase fluctuations at all orders as in the case of incoherently driven exciton polaritons described in [16]. For small decay rates and to leading order in the photon field, the mean-field equation for the case where the two-level systems are resonant with the $k = 0$ photon mode and pumped at the lower polariton may be approximated by the cavity response relation

$$f = -4g\psi_\mathrm{f}|\psi_\mathrm{f}|^2. \tag{6.16}$$

Figure 6.1 shows how the Keldysh saddle point result for the coherent field compares with the semiclassical result. The two results do not match perfectly, but deviations at small drive strength are small. The discrepancy is not unexpected given that the two approaches implement different Hamiltonians: The Keldysh approach splits the two-level systems into fermionic degrees of freedom a and b whose constraint $a^\dagger a + b^\dagger b = 1$ is imposed on average, but not exactly at the microscopic level [64]. Additionally, the dissipative terms associated with a and b differ from the Lindblad form described in previous chapters in that each of the fermionic degrees of freedom is coupled to a

[2]The denominator is equivalent to (the maybe more familiar expression) $\left((\nu - E)^2 + \gamma^2\right)\left((\nu + E)^2 + \gamma^2\right)$.

separate decay bath.

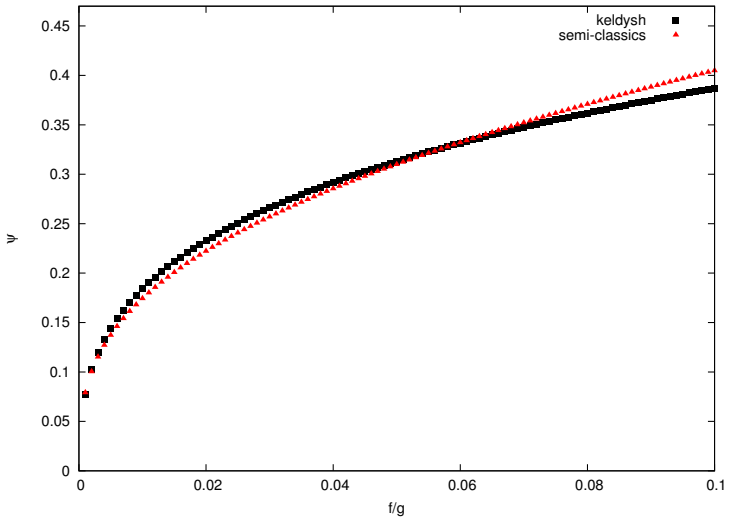

Figure 6.1: Comparison of the Keldysh and semiclassical photon expectation values $\psi = |\langle a \rangle|$ as a function of drive strength. The match is not perfect, but very good.

6.2 Fluctuations and luminescence

The luminescence spectrum can be determined from the photon Green function. By expanding about the saddle point, $G^{-1} = G_{\mathrm{sp}}^{-1} + \delta G^{-1}$, and writing the inverse photon Green function D^{-1} in the basis

$$\begin{pmatrix} \psi_{\mathrm{cl}}(k,\omega) \\ \psi_{\mathrm{cl}}^{\dagger}(-k,-\omega) \\ \psi_{\mathrm{q}}(k,\omega) \\ \psi_{\mathrm{q}}^{\dagger}(-k,-\omega) \end{pmatrix} \tag{6.17}$$

one can find the self-energies as convolutions of pairs of components of G, corresponding to a single loop approximation. Integration is possible via the residue theorem, and summing over the appropriate residues symbolically in

Mathematica we obtain inverse photon Green functions of the form

$$\left(D^{-1}\right)^R = \begin{pmatrix} K_1(\omega) & K_2(\omega) \\ K_2(-\omega)^* & K_1(-\omega)^* \end{pmatrix} \tag{6.18}$$

$$\left(D^{-1}\right)^K = \begin{pmatrix} L_1(\omega) & L_2(\omega) \\ -L_2(\omega)^* & L_1(-\omega) \end{pmatrix}. \tag{6.19}$$

Inverting these, once again symbolically in Mathematica, one can find

$$\mathcal{S} = \frac{i}{2}\left[D^K(1,1) - \left(D^R(1,1) - D^A(1,1)\right)\right] \tag{6.20}$$

in terms of the different photon Green functions, which can be shown to be equal to the luminescence spectrum.

The spectra found in the Keldysh approach are not the same as those in the previous chapter. This is because we previously calculated the single-cavity fluctuations, whereas the Keldysh approach treats fluctuations in the delocalised $k = 0$ Fourier mode. Additionally, the Keldysh spectra do not take into account the possibility of $k = 0$ fluctuations consisting of pairs of non-zero momentum fluctuations that add up to zero. Specifically, it is possible for higher order correlation functions to allow excitations where at least two pairs of momenta add up to a $k = 0$ excitation, which may then be occupied by D^K. Such correlation effects may be assumed to be particularly strong at small bandwidth and require a treatment beyond linearised fluctuation theory.

It is possible to analyse the zeros of the inverse retarded Green function in the limit of $\gamma, \kappa \to 0$ and small ψ analytically. The locations of the fluorescence peaks are given by $\pm\left(2g - g|\psi_\mathrm{f}|^2\right)$ and $\pm 2\sqrt{2}g|\psi_\mathrm{f}|^2$. The full spectrum is shown in figure 6.2. It shows the four peaks described by the retarded Green function, as well as a zero frequency peak. In addition to an elastic peak, there is a finite-width occupation at $\omega = 0$. As there is no pole in D^R at $\omega = 0$, this is purely an occupation effect described by the Keldysh Green function.

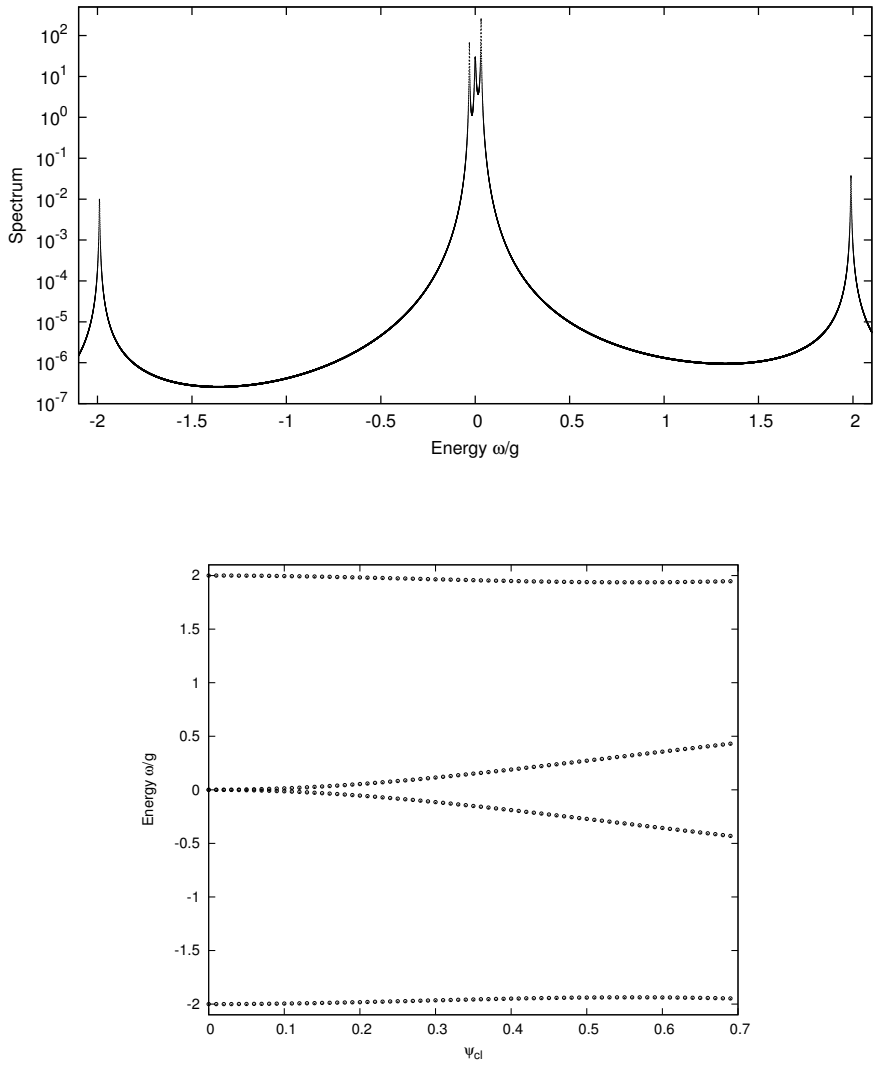

Figure 6.2: Top panel: Zero momentum spectrum as calculated in the Keldysh approach. The spectrum is different from that of the mean-field approach, as explained in the text. Bottom panel: Zeros of the inverse retarded Green function as a function of the (classical) coherent field.

Chapter 7

Time-Evolving Block Decimation

Going beyond mean-field theory in the small hopping limit can be achieved by time-evolving block decimation. As described in the introduction, this is a method of systematically eliminating degrees of freedom in the entanglement between the sites that are of no or little relevance to the physics.

7.1 Implementation

Using the same notation as in the introduction, we express the density matrix ρ as a product of on-site matrices Γ and diagonal bond matrices Λ of dimension χ-by-χ. In order to make the problem tractable, we use the spin-chain Hamiltonian and density matrix equation described in equation (5.4). For each site, there are $d = 4$ Γ matrices — the 2-dimensional Hilbert space gives rise to four degrees of freedom in the density matrix, which we will express in terms of the Pauli basis $\{I, \sigma^x, \sigma^y, \sigma^z\}$.

As the initial state we choose the empty state $(I - \sigma^z)/2$. Like in many of the more recent publications on time-evolving block decimation, we make a small modification to the singular value decomposition step of the time-evolution: After applying the evolution operator P, we do not perform the decomposition on the matrix $P\Gamma^{j_L}\Lambda^L\Gamma^{j_{L+1}}$. Instead we decompose

$\Lambda^{L-1}P\Gamma^{j_L}\Lambda^{L}\Gamma^{j_{L+1}}\Lambda^{L+1}$, discard all but the first χ singular values, and then pre- and post-multiply the resulting new Γ matrices by the inverse matrices $\left[\Lambda^{L-1}\right]^{-1}$ and $\left[\Lambda^{L+1}\right]^{-1}$, respectively. This is known to improve the stability of the algorithm. The matrix inversion is performed numerically by imposing a cutoff on the bond matrix values.

Our system of choice consists of ten cavities with open boundary conditions. Near the end points of the chain we restrict the bond dimension χ to d^L at distance L from the nearest boundary, in line with the maximum possible entanglement between states.

7.2 Results

As in the mean-field calculation in Chapter 5, the focus of our analysis is the calculation of the photon expectation value $|\langle a \rangle|$ as a function of pump frequency μ. In particular, we are interested in the region of the anti-resonance and bistability in a chain of cavities beyond mean-field theory.

Our implementation uses a chain of ten cavities with open boundary conditions and coherent drive and dissipation on each site as described previously. Unlike in the mean-field calculation, we no longer use the on-site field to represent the effect of an infinite number of nearest neighbours. Instead even for bond dimension $\chi = 1$ corresponding to only classical correlations between cavities, it is the two adjacent sites' field that is seen by each cavity. Due to the finite length of the chain, homogeneity along the chain is lost. We thus study the photon field in the central cavities.

In addition to these differences between the mean-field calculation of Chapter 5 and this finite system, we expect the quantum mechanical correlations between sites to have a significant effect: In particular, where previously the system showed bistability by self-consistently evolving in time towards one of two different steady state density matrices, we now expect only one steady state density matrix with a bimodal probability distribution. This is because the full density matrix of the entire system is an ensemble average over all states and is as such single-valued. There is thus only one steady state density matrix replacing the self-consistency condition of mean-field

theory.

The numerical calculation is performed by time-evolving the density matrix within TEBD until a steady state is reached. This is done for a range of drive frequencies, and the previous calculation's steady state is used as the initial condition for the calculation at the next drive frequency. Figure 7.1 shows the results of this calculation for two different values of hopping J. Most notably, the anti-resonant feature persists with quantitative modifications as quantum correlations between sites are included in the calculation. As the entanglement between sites grows with increasing hopping, a small bond dimension can only describe the small hopping limit.

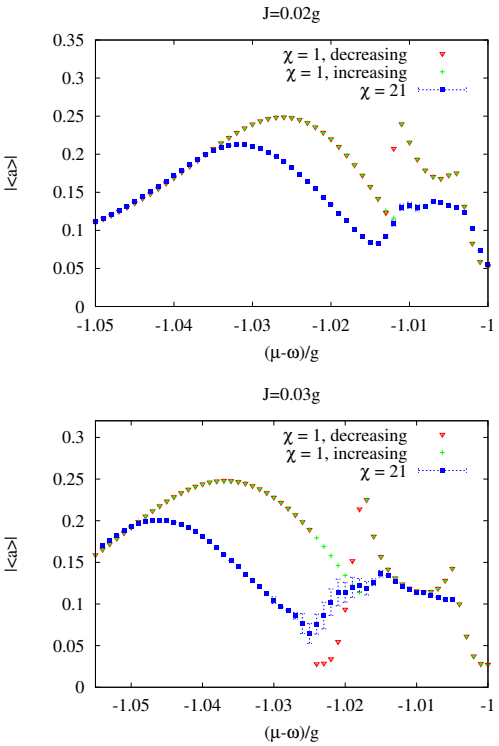

Figure 7.1: Expectation value of the photon operator in one of the two central cavities as a function of pump frequency for two different values of hopping J. We use the steady state of the time evolution at the previous pump frequency as initial conditions for the next pump frequency. For bond dimension $\chi = 1$ this gives rise to bistability, which is shown by plotting the expectation values for both increasing and decreasing drive frequencies.

Photon expectation value Figure 7.1 shows the steady state values of the coherent photon field as a function of pump frequency for values of hopping $J = 0.02g$ (at the onset of bistability in the mean-field calculation) and $J = 0.03g$ (in the bistable regime in the mean-field calculation). As the truncation of the Schmidt coefficients can introduce small errors at every time step, figure 7.1 includes error bars for points where the error was larger than the point size. These small errors can also slightly break the symmetry between odd and even sites.

For bond dimension $\chi = 1$, corresponding to only classical ('mean-field-like') correlations between sites, the overall anti-resonant feature along with a region of bistability are preserved. However, due to the loss of homogeneity, additional features appear even without quantum correlations. For $\chi = 21$, many of the sharp features are lost, although the overall anti-resonance is still present.

Unlike the anti-resonance, the bistable behaviour that was present in the infinite system within mean-field theory has disappeared from the $\chi = 21$ results. This is not surprising, as one would expect the bistable behaviour to turn into bimodality in the full quantum system: There can only be one density matrix of the full quantum system, which is determined by an ensemble average over all states. In the mean-field calculation, the self-consistent determination of the (effectively single-site) density matrix allowed two different steady state solutions. In the full quantum treatment, these solutions turn into weighted components of the full density matrix.

For bimodality, one would expect a strongly mixed quantum state. This is indeed present, as can be deduced from the magnitude of the Bloch vector of the single site density matrix shown in figure 7.2. Here, we write the single site density matrix in Pauli matrix components as $\rho = \frac{1}{2}(I + \vec{s}\cdot\vec{\sigma})$ with the Bloch vector $\vec{s}$. In this notation, the magnitude of $\vec{s}$ in the xy plane, $s = \sqrt{(s^x)^2 + (s^y)^2}$, determines the photon expectation value $|\langle a\rangle|$. The anti-resonance and the location of the bistability within mean-field theory mark a region where the otherwise pure (coherent) state becomes significantly mixed, which corresponds to low coherence but large occupation. However, even the mean-field calculation gives rise to mixed states as entanglement with the

environment gives rise to loss of coherence.

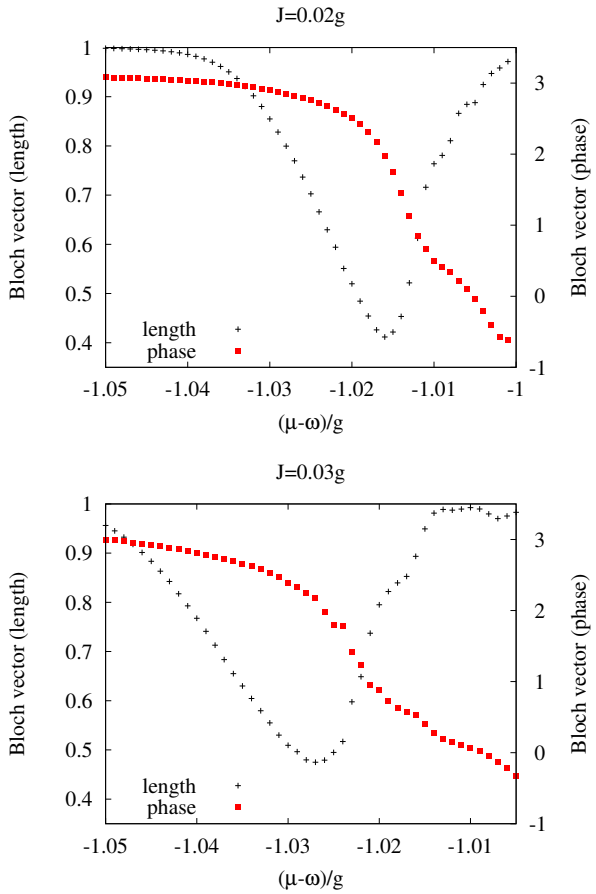

Figure 7.2: Length and phase of the Bloch vector for $\chi = 21$. The transition from a pure to a mixed and back to a pure state is clearly visible.

Full state tomography In addition to the eigenvalues of the density matrix represented by the magnitude of the Bloch vector, one can extract phase information, allowing us to perform full state tomography of the single site density matrix. Figure 7.2 also shows the phase of the Bloch vector in the xy plane, $\arctan \frac{s^y}{s^x}$, over the same range of pump frequencies μ. Across the resonant and anti-resonant features the phase changes rapidly as expected near a resonance.

In order to investigate further the nature of the steady state density

matrix, one may analyse the Wigner quasi-probability distribution

$$W(\alpha,\alpha^*) = \frac{1}{\pi^2}\int \mathrm{d}^2\beta e^{-i(\beta\alpha^*+\alpha\beta^*)}\mathrm{tr}\left(e^{i(\beta a^\dagger+\beta^* a)}\rho\right) \tag{7.1}$$

for signatures of bimodality. Here, ρ is the density matrix in the full bosonic Hilbert space. By only considering states within the restricted (spin-chain) Hilbert space, one can show that the Wigner distribution becomes

$$\begin{aligned} W(\alpha,\alpha^*) &= \frac{2}{\pi}\int_0^\infty \mathrm{d}x\left[\left(1-\frac{x^2}{2}(1-s^z)\right)xe^{-x^2/2}\,\mathrm{J}_0(2|\alpha|x)\right] &(7.2)\\ &- \frac{1}{\pi}s\cos(\theta-\tau)\int_0^\infty \mathrm{d}x\left[x^2e^{-x^2/2}\,\mathrm{J}_1(2|\alpha|x)\right]. &(7.3)\end{aligned}$$

Here, θ and τ are the phase angles of the Bloch vector in the xy plane and of α, respectively. s^z is the σ^z component of the steady state density matrix and s is the length of the Bloch vector in the xy plane. The angular integrals in equation (7.1) give rise to the Bessel functions J_0 and J_1.

As the space of single site states is only spanned by the two states of the effective two-level system, and as the mixed states are possible simply through entanglement with the environment, the Wigner function does not provide significant information beyond what is encoded in the eigenvalues of the density matrix (or the Bloch vector, respectively). In particular, it does not confirm bimodality. In order to fully understand bimodality, one would need to study correlations between sites, as these correlations induce the bistable behaviour through self-consistency in the mean-field calculation and the suspected bimodal behaviour in the case of the full (or within TEBD approximate) quantum system. For completeness, the on-site Wigner distribution is shown in figure 7.3.

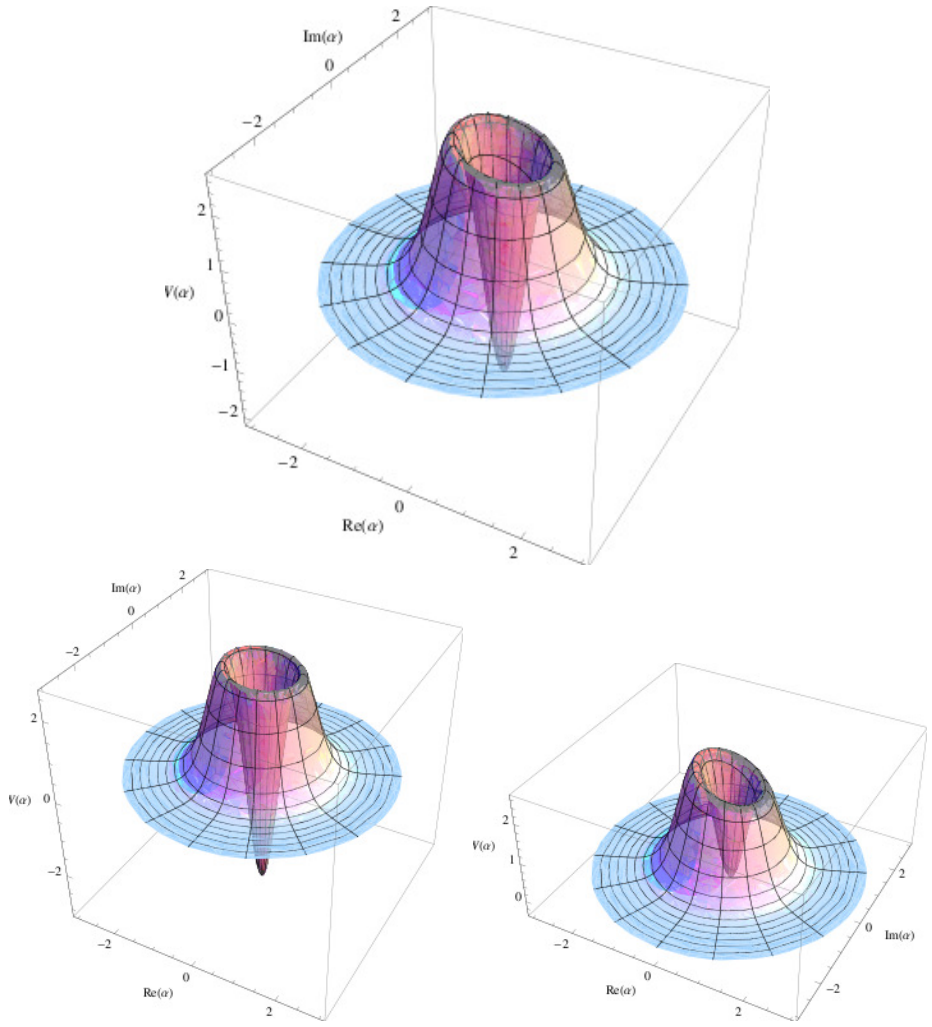

Figure 7.3: Top panel: On-site Wigner distribution corresponding to the $J = 0.03g$, $\chi = 21$ parameter set used in the previous two figures at $(\mu - \omega)/g = -1.021$ [$s^x = 0.0946$, $s^y = 0.1317$, $s^z = -0.3310$]. Bottom panels: Corresponding Wigner distributions obtained for the two steady state solutions for $J = 0.03g$ and $\chi = 1$. [Bottom-left panel: decreasing μ, $s^x = -0.0053$, $s^y = 0.0776$, $s^z = -0.4939$. Bottom-right panel: increasing μ, $s^x = -0.1357$, $s^y = 0.1582$, $s^z = -0.0484$.] The distributions are akin to number states with weak phase dependence. By eye, the $\chi = 21$ distribution looks like a combination of the two $\chi = 1$ solutions.

Part III

Linewidth Narrowing of Qubits in a Cavity

Chapter 8

Several Qubits in a Cavity

In this chapter we study decay processes in a strongly coupled quantum optical system. With light-matter coupling being large compared with the energy scale on which the density of states of the dissipative environment varies, we find that the correct treatment involves the determination of decay rates for the system eigenmodes, rather than for its light and matter constituents separately. Specifically, we investigate the transmission spectrum of a set of qubits coupled strongly to a single cavity. We show that for $1/f$ noise the dephasing-dominated linewidth can both increase and decrease with qubit number, depending on the number of qubits and whether all qubits couple to a single or separate dephasing baths. Experiments[1] have seen a decrease in the linewidth of the collective Rabi peaks of qubits coupled to a microwave resonator as the number of qubits is increased from one to three. This effect is surprising as a naïve Master equation calculation of phase evolution and separate Lindblad terms for photons and qubits can only give rise to a constant or increasing linewidth. The experiments were done in the limit where dephasing was the dominant decay channel and the system was weakly driven.

As discussed in the introduction the dissipative coupling of N qubits to external environments may, under certain idealised conditions, be described

[1] performed by Johannes Fink at ETH Zurich, published in [3]

by Lindblad terms in the equation of motion of the system density matrix,

$$\dot{\rho} = -i[H, \rho] + \mathcal{D}. \tag{8.1}$$

The decay term $\mathcal{D}$ in the problem at hand is given by $\mathcal{D} = \frac{\gamma_\parallel}{2} \sum_i \mathcal{L}[\sigma_i^z] + \frac{\gamma_\perp}{2} \sum_i \mathcal{L}[\sigma_i^-]$ if each qubit couples independently to a separate environment, or by $\mathcal{D} = \frac{\gamma_\parallel}{2} \mathcal{L}[\sum_i \sigma_i^z] + \frac{\gamma_\perp}{2} \mathcal{L}[\sum_i \sigma_i^-]$ in the case where collective system operators $\sum_i \sigma_i$ couple jointly to a single environment. The corresponding total linewidths are $\left(2\gamma_\parallel + \frac{\gamma_\perp}{2}\right)$ and $\left(2\gamma_\parallel + N\frac{\gamma_\perp}{2}\right)$, respectively. The factor of N enhancing the linewidth in the collective case arises due to constructive interference of different decay pathways. This effect is related to that of superradiant emission of light from a collection of spins prepared in their excited states [65]. Constructive interference between the individual spins constituting a collective symmetric state enhances the emission probability of photons.

The idea of our approach is to re-derive an effective equation of motion for the system (qubits and cavity) by tracing out the bath degrees of freedom. However, we need to account for the strong coupling of light and matter degrees of freedom first and find decay terms for the actual eigenmodes of the system [66]. These eigenmodes determine the frequencies at which the decay baths are sampled and hence affect the effective decay rates in the context of frequency-dependent noise. As transitions between eigenstates scale with the collective Rabi frequency, which increases with qubit number, the effective dephasing rate is expected to decrease. The decay terms in this approach are naturally obtained in terms of the system's eigenstates, rather than added Lindblad operators added to the density matrix equation of motion *ad hoc*. The importance of phrasing problems involving open strongly coupled systems in terms of their eigenstates was pointed out for the Jaynes-Cummings model by [36]. Experiments on quantum dots [67, 68] have seen the frequency dependence of sampling a dephasing bath (in this case longitudinal acoustic phonons) with a non-trivial density of states.

8.1 Born-Markov approximation and secularisation procedure

In order to describe the effect of the baths on the density matrix of the strongly-coupled system, we follow the Bloch[69]-Redfield[70] approach. Like in Part I, we will make a Born-Markov approximation. In order to preserve positivity of the density matrix we will then secularise the decay terms.[2]

Ultimately we wish to find the transmission spectrum of the cavity, $\langle a^\dagger a \rangle$ as a function of pump frequency. Working at very low pump powers, corresponding to the linear response regime, we can neglect the coherent pump term for now and work with the Hamiltonian operators $H = H_{\rm sys} + H_{\rm baths} + H_{\rm int}$ describing the system, a separate free bosonic bath for each qubit, and the coupling between those two terms. We will later investigate the difference between each qubit being coupled to a separate dephasing bath, as compared with all qubits coupling collectively to a single bath. Using the Hamiltonians

$$H_{\rm sys} = \omega a^\dagger a + \sum_{i=1}^{N} \frac{\epsilon_i}{2}\sigma_i^z + \sum_{i=1}^{N} g_i \left(\sigma_i^+ a + \text{h.c.}\right) \tag{8.2}$$

$$H_{\rm int} = \sum_{i,q} \gamma_q \left(\frac{\sigma_i^z}{2}\right)\left(b_{iq}^\dagger + b_{iq}\right) \tag{8.3}$$

$$H_{\rm baths} = \sum_{iq} \beta_{iq} b_{iq}^\dagger b_{iq} \tag{8.4}$$

the coupling to baths describes dephasing (i.e. coupling the z-component of each of the spins to a separate bosonic freely-evolving bath).

As a first step, we transform to the interaction picture,

$$\tilde{H}_{\rm int} = \sum_i P_i(t)\Phi_i(t) \tag{8.5}$$

$$P_i(t) = e^{iH_{\rm sys}t}\left(\frac{\sigma_i^z}{2}\right)e^{-iH_{\rm sys}t} \tag{8.6}$$

$$\Phi_i(t) = \sum_q \gamma_q \left(b_{iq}^\dagger e^{-i\beta_{iq}t} + \text{h.c.}\right). \tag{8.7}$$

[2] i.e. we eliminate in the interaction picture the time-dependence of the decay terms

and formally integrate the von Neumann equation of motion for the density operator

$$\dot{\rho} = -\mathrm{tr}_{\mathrm{R}} \int_{-\infty}^{t} \mathrm{d}t' \left[H_{\mathrm{int}}, \left[H_{\mathrm{int}}, \rho\right]\right]. \tag{8.8}$$

The decay baths have correlation functions

$$\langle \Phi_i(t)\Phi_j(t')\rangle = \int_{-\infty}^{\infty} \mathrm{d}\nu J(\nu) \left[(n(\nu)+1)e^{-i\nu(t-t')} + n(\nu)e^{i\nu(t-t')}\right] \delta_{ij} \tag{8.9}$$

with $J(\nu) \propto \Theta(\nu)/\nu$. $n(\nu)$ are the occupation functions of the bosonic baths and we define the terms in square brackets to be $f_\nu(t-t')$. The trace over bath degrees of freedom can now be converted into integrals, giving

$$\begin{aligned}\dot{\rho} = -\sum_{i=1}^{N} \int_{-\infty}^{\infty} \mathrm{d}\nu J(\nu) \int_{-\infty}^{t} \mathrm{d}t' \left(\left[P_i(t)P_i(t')\rho(t) - P_i(t')\rho(t)P_i(t)\right] f_\nu(t-t')\right. \\ \left. + \left[-P_i(t)\rho(t)P_i(t') + \rho(t)P_i(t')P_i(t)\right] f_\nu(t'-t)\right)\end{aligned} \tag{8.10}$$

Here, we have made use of the Born-Markov approximation leaving the reservoirs unaffected by the system and eliminating any time non-local effects mediated by the baths. This amounts to a perturbative calculation similar to that described in Part I.

The time-integrals can be performed analytically, whereas the integration over frequency can only be done numerically due to the non-trivial terms $J(\nu)$ and $n(\nu)$. However, introducing projection operators onto energy eigenstates

of the system Hamiltonian (denoted by Greek letters)

$$\begin{aligned}
&\int_{-\infty}^{t} \mathrm{d}t' \int_{-\infty}^{\infty} \mathrm{d}\nu\, \Pi_\gamma\, P_i(t') f_\nu(t-t') \Pi_\delta \\
&= |\gamma\rangle\langle\gamma|\sigma_i^z|\delta\rangle\langle\delta| \left(\pi(n(E_\delta - E_\gamma)+1) J(E_\delta - E_\gamma) - i\mathcal{P} \int_{-\infty}^{\infty} \mathrm{d}\nu \frac{(n(\nu)+1)J(\nu)}{\nu + E_\gamma - E_\delta} \right. \\
&\left. + \pi n(E_\gamma - E_\delta) J(E_\gamma - E_\delta) + i\mathcal{P} \int_{-\infty}^{\infty} \mathrm{d}\nu \frac{n(\nu) J(\nu)}{\nu - E_\gamma + E_\delta} \right) e^{-i(E_\delta - E_\gamma)t} \\
&\equiv |\gamma\rangle\langle\gamma|\sigma_i^z|\delta\rangle\langle\delta| \left(A_{\delta\gamma} - iB_{\delta\gamma}\right) e^{-i(E_\delta - E_\gamma)t}
\end{aligned} \tag{8.11}$$

we see that the terms separate into real and imaginary (or δ-function and principal value) parts. The direct application of the Born-Markov approximation does not yield decay terms of Lindblad form, and thus violates positivity of the density matrix. It is known [13] that the exclusion of all terms with a time-dependence in the interaction picture recovers the correct Lindblad form. As a result, we find two contributions towards the dephasing channel, $\dot{\rho}_{\mathrm{dephasing}} = \mathcal{L}_{\mathrm{d}} + i[H_{\mathrm{s}}, \rho]$: a set of decay terms in Lindblad form ($\mathcal{L}_{\mathrm{d}}$) and a phase evolution ($i[H_{\mathrm{s}}, \rho]$) due to an effective Hamiltonian shift, which we may view as a Lamb shift. Absorbing various constants, these are

$$\mathcal{L}_{\mathrm{d}} = -\sum_{i\alpha\beta\gamma\delta} \left(2 r_{\gamma\delta} \rho r^\dagger_{\beta\alpha} - r^\dagger_{\beta\alpha} r_{\gamma\delta} \rho - \rho r^\dagger_{\beta\alpha} r_{\gamma\delta} \right) \delta(E_\alpha - E_\beta + E_\gamma - E_\delta). \tag{8.12}$$

and

$$\mathcal{L}_{\mathrm{s}} = i[H_{\mathrm{s}}, \rho] \tag{8.13}$$

$$\begin{aligned}
H_{\mathrm{s}} &= \sum_{i\alpha\beta\gamma\delta} \left[B_{\alpha\beta} |\alpha\rangle\langle\alpha| \left(\frac{\sigma_i^z}{2}\right) |\beta\rangle\langle\beta||\gamma\rangle\langle\gamma| \left(\frac{\sigma_i^z}{2}\right) |\delta\rangle\langle\delta| \right] \delta(E_\alpha - E_\beta + E_\gamma - E_\delta) \\
&= \sum_{i\alpha\beta\delta} \left[B_{\alpha\beta} |\alpha\rangle\langle\alpha| \left(\frac{\sigma_i^z}{2}\right) |\beta\rangle\langle\beta| \left(\frac{\sigma_i^z}{2}\right) |\delta\rangle\langle\delta| \right] \delta(E_\alpha - E_\delta).
\end{aligned} \tag{8.14}$$

The $r^i_{\alpha\beta}$ are re-scaled spin components in the energy basis,

$$r^i_{\alpha\beta} = \sqrt{A_{\alpha\beta}}|\alpha\rangle\langle\alpha|\left(\frac{\sigma^z_i}{2}\right)|\beta\rangle\langle\beta|. \tag{8.15}$$

By combining terms in equation (8.12), it can be shown that this is of Lindblad form and hence preserves positivity. Considering the entire sum in equation (8.14), it is easy to see that the effective Hamiltonian is hermitian as required.

8.2 Implementation

The full equation of motion, of which we wish to find the steady state, is

$$\dot{\rho} = -i[H_{\text{sys}}, \rho] + \kappa\mathcal{L}[a] + \gamma\mathcal{L}_{\text{d}} + i\gamma[H_{\text{s}}, \rho] \tag{8.16}$$

where $\mathcal{L}[a]$ is a photon decay term with small decay rate κ.

The overall scale of the dephasing bath density of states $J(\nu)$ is a priori unknown and thus determined from the (experimental) linewidth of a single qubit by fitting the parameter γ. The fitting procedure is performed by using the value of γ as an input parameter for our calculation and iteratively approaching the value of γ which is consistent with the experimental linewidth.

We implement the equation of motion in Matlab, writing the right-hand side as a superoperator $\rho^{\#}$. The Hilbert space for N qubits in a cavity is restricted to $(N+2)$ dimensions (empty state, single photon, each of the spin-up states with no photons), giving rise to an $(N+2)^2$-by-$(N+2)^2$ superoperator, of which we find the steady state as the eigenvector corresponding to the zero eigenvalue. This restriction to $N+2$ states is justified for weak drive strength.

In the linear response regime (weakly driven — the pump is added to the Hamiltonian as $f(a^\dagger + a)$) we only need to calculate the decay terms at a single pump frequency as they only depend on energy differences, which are unaffected by shifts in the pump frequency.

The problem involves almost degenerate energy levels which can cause numerical issues when solving the density matrix equation of motion. In order to correctly implement the δ-function constraint on allowed transitions, we need to allow for numerical errors without introducing any time dependence in the interaction picture. This turns out to work best by choosing $|E_\alpha - E_\beta + E_\gamma - E_\delta| < \min_{\forall E_i \neq E_j} |E_i - E_j|$, i.e. choosing the smallest possible transition between energy levels as the cutoff. This choice seems robust against numerical errors. Furthermore, better numerical stability is achieved by initially diagonalising the $(N+1)$-by-$(N+1)$ Hamiltonian that excludes the vacuum state and adding the empty state (which is only coupled through the pump term) at the end.

The occupation function $n(\nu)$ is a Bose-Einstein distribution at very low temperature, but most of our results were obtained for zero temperature corresponding to empty decay baths, as experimentally $k_B T \ll g$. At low frequency the bath density of states $J(\nu)$ and the occupation function $n(\nu)$ need to be cut off to avoid divergences in our numerical calculation. We take them smoothly to zero over a small range. The exact choice of range does not affect the numerical results. Any principal values of the form $\frac{1}{\nu - x}$ are smoothed by using $\mathrm{Re}\frac{1}{\nu - x + i\epsilon}$ for very small ϵ.

8.3 Results

Using the implementation described in the previous section, we find the photon response to weak driving as $\langle a^\dagger a \rangle$ as a function of pump frequency. The calculation shown above assumes that all qubits couple individually to separate dephasing baths. The calculation for the case where all qubits couple

collectively to a single decay bath is analogous: We simply use

$$H_{\text{sys}} = \omega a^\dagger a + \sum_{i=1}^{N} \frac{\epsilon_i}{2}\sigma_i^z + \sum_{i=1}^{N} g_i \left(\sigma_i^+ a + \text{h.c.}\right) \tag{8.17}$$

$$H_{\text{int}} = \sum_q \gamma_q \left(\sum_i \left(\frac{\sigma_i^z}{2}\right)\right)\left(b_q^\dagger + b_q\right) \tag{8.18}$$

$$H_{\text{baths}} = \sum_q \beta_q b_q^\dagger b_q, \tag{8.19}$$

replace equation (8.6) by

$$P(t) = e^{iH_{\text{sys}}t}\left(\sum_i \left(\frac{\sigma_i^z}{2}\right)\right)e^{-iH_{\text{sys}}t} \tag{8.20}$$

and take the summation signs relating to sums over qubits i in all subsequent equations inside the corresponding terms.

As shown in Figure 8.1, the linewidth decreases monotonically with qubit number when the coupling is collective, whereas there is an increase followed by a decrease when all qubits are coupled individually to separate baths. A heuristic explanation for this behaviour is as follows: With increasing number of qubits we always expect the linewidth to decrease as $1/\sqrt{N}$ (because the transition energies scale as $\sqrt{N}$). However, when each qubit dephases individually, the number of decay channels increases as N because the eigenstates are delocalised over all qubits and so every eigenstate couples to every decay bath. This gives rise to an initial increase in the effective decay rate (linewidth).

For all these calculations we have used a value of 1 for spin operators in the excited state and 0 in the ground state. This is to ensure a trace that does not grow with qubit number in the restricted Hilbert space we are working in. The energy shift due to this transformation is negligible as discussed in the appendix (section 8.5), but was included for completeness in the numerical calculations.

Figure 8.2 shows a comparison with the experimental results. The only fit parameter used was the coupling strength γ, which was calculated for the

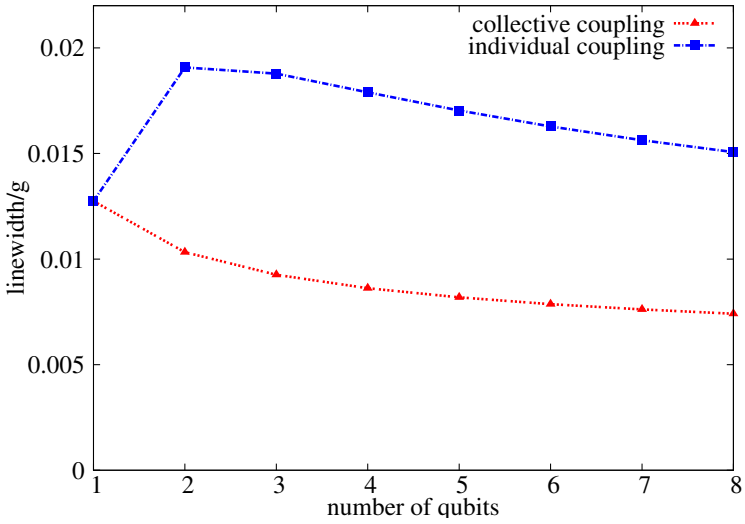

Figure 8.1: Linewidths of the cavity-qubit system for N qubits (theoretical results for individual and collective coupling to baths).

one qubit ($N = 1$) case and kept the same for $N = 2, 3$.

By varying the detuning between a single qubit and the cavity mode, we can investigate the effect of the dephasing in more detail. For a single qubit coupled to the photon mode, the eigenstates without pump and decay are upper and lower polaritons. As the detuning is varied through resonance, we expect a shift towards the photon and qubit weights for the respective polaritons. However, an additional effect should be visible (and in fact dominant) in the spectrum: As the decay is largely due to dephasing with the purely photonic linewidth being significantly smaller, a polariton with large photon weight should have a small linewidth (and saturate at the bare cavity linewidth). Equally, the linewidth should decrease for the qubit-dominated polariton as it samples the decay bath at a Rabi frequency that is increased by the presence of the detuning, $\sqrt{g^2 + \Delta^2}$ rather than g for detuning Δ. As a result we see in figure 8.3 that the linewidth is near its maximum on resonance and decreases towards both positive and negative detuning.

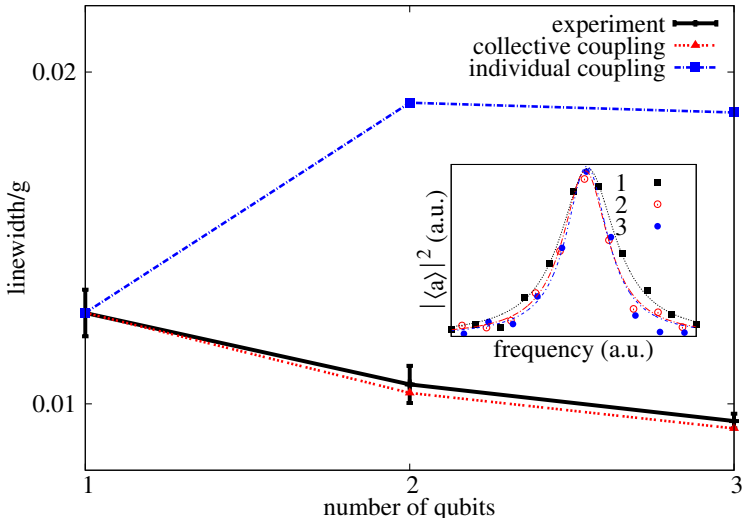

Figure 8.2: Linewidths of the cavity-qubit system for one, two and three qubits (comparison between experiment and theory). The inset shows the experimental results with Lorentzian fits for comparison by eye. Experiments by Johannes Fink and Andreas Wallraff [3].

8.4 Scaling of peak height and two-level model

The entire calculation described above is only valid in the linear response regime, i.e. when the drive strength is small enough for the energy levels to be unaffected and the two-level systems not to be saturated.[3] Beyond linear response, when saturation effects become important, one would expect power broadening of the Rabi peaks. We can determine the scaling of the peak heights and linewidths using an analytical model for a single qubit in a cavity. The undriven system Hamiltonian for 0 and 1 excitations is

$$\begin{aligned} H &= \frac{\epsilon}{2}\sigma^z + \omega a^\dagger a + g\left(\sigma^+ a + \text{h.c.}\right) \\ &= \begin{pmatrix} \frac{\epsilon}{2} & g & 0 \\ g & \omega - \frac{\epsilon}{2} & 0 \\ 0 & 0 & -\frac{\epsilon}{2} \end{pmatrix} \end{aligned} \tag{8.21}$$

[3]For large drive strength there may be a non trivial interaction between the drive and dissipation terms.

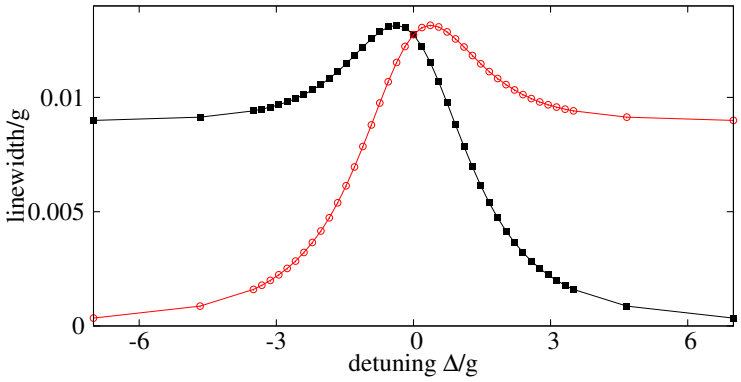

Figure 8.3: Linewidths obtained from Lorentzian fits for a single qubit in a cavity as a function of qubit-cavity detuning. The linewidths of positive and negative frequency peaks (corresponding to upper and lower polaritons) cross over at zero detuning. The large-$|\Delta|$ asymptotes correspond to the bare cavity decay rate and the sampling of the dephasing bath at increasing collective Rabi frequency, $\sqrt{g^2+\Delta^2}$.

which can be diagonalised by means of a unitary transformation,

$$H = \begin{pmatrix} E_+ & 0 & 0 \\ 0 & E_- & 0 \\ 0 & 0 & 0 \end{pmatrix} - \frac{\epsilon}{2}\mathrm{I}. \tag{8.22}$$

The diagonal entries are the polariton states and the empty state, respectively. In the frame rotating at the pump frequency, these are replaced by $E_\pm \to E_\pm - \mu$. We can now project onto the polariton state that is close to the pump frequency in order to obtain a two-level system consisting of one polariton and the empty state. Adding a photon pump term, we have

$$H = \begin{pmatrix} \delta & f\sin\theta \\ f\sin\theta & 0 \end{pmatrix} \tag{8.23}$$

where θ is the rotation angle of the unitary transform, and δ is the detuning between polariton and pump energies. When the qubit is (nearly) resonant

with the cavity, we have (approximately) $\sin\theta = 1/\sqrt{2}$. The steady state of the equation of motion is now determined by

$$\begin{aligned}\dot{\rho} &= -i[H,\rho] + \kappa\left(2a\rho a^\dagger - a^\dagger a\rho - \rho a^\dagger a\right) + \gamma\left(2\sigma^z\rho\sigma^z - \sigma^z\sigma^z\rho - \rho\sigma^z\sigma^z\right) \\ &= 0 \end{aligned} \tag{8.24}$$

where we have assumed some effective dephasing rate γ determined by the linewidth. Solving for the steady-state components of the density matrix, we find that

$$\langle a\rangle = \frac{f^2}{\sqrt{2}\kappa\gamma}\left(\frac{\gamma^2}{\gamma^2+\delta^2}\right) \tag{8.25}$$

given $f < \kappa < \gamma$ (dephasing is the dominant decay channel; weak drive being the characteristic feature of the linear response regime). This relates the peak height (first term) to the linewidth (γ — the term in brackets is a Lorentzian normalised to a height of 1). Our numerical results confirm this relation, suggesting that no power broadening occurs.

8.5 Appendix: Energy shift due to spin transformation

In the $(N+2)$-by-$(N+2)$ basis (all up-spins, down-spin with one photon, empty state), the trace of the spin operators grows with the number of qubits. In the following, we will show that there is a resulting shift to the qubit energies on the order of the Lamb shift — which is tiny and has no significant effect on the linewidths. The importance of this analysis lies in the saturation of the trace of the operators involved in the decay and dephasing processes. Representing the spin operators in this basis, for the collective case, the traces of both $\left(\sum_i(\sigma_i^z/2)\right)^2$ and $\left(\sum_i(\sigma_i^z/2)\right)$ grow as N. Naïvely representing spins as $\mathrm{diag}(1/2,-1/2,-1/2,...)$ would have led to traces growing as $N^3/4 - N^2/2 + N$ and $-N^2/2$, respectively. Since $\sum_{ab}|\langle a|\sum_i(\sigma_i^z/2)|b\rangle|^2 = \mathrm{tr}\left(\sum_i(\sigma_i^z/2)\right)^2$, the trace of the square of the collective spin operator indicates the scaling of the matrix elements, demonstrating that we expect a saturation in the dephasing contribution from the matrix elements.

As the trace of spin operators in the $(N+2)$-by-$(N+2)$ basis grows with qubit number, which would increase not only the number but also the weights of the decay channels, we use an alternative representation: By adding a multiple of the identity, we obtain spin operators of the form

$$\mathrm{diag}(1,0,0,...),\ \mathrm{diag}(0,1,0,...),\ .... \tag{8.26}$$

These have unit trace (irrespective of the size of the Hilbert space). The corresponding transformation is

$$\begin{aligned} \sigma_i^z &\rightarrow (|e_i\rangle\langle e_i| - |g_i\rangle\langle g_i|) + I_{\mathrm{TLS}} \\ &= 2\,|e_i\rangle\langle e_i| \end{aligned} \tag{8.27}$$

where I_{TLS} denotes the identity matrix in the Hilbert space of two-level systems.

The term in equation (8.27) that is proportional to the identity matrix has no effect in the system Hamiltonian as it constitutes a constant shift in energy. However, in the interaction Hamiltonian, we get a resulting shift by

$$-\sum_{iq}\gamma_q\left(b_{iq}^\dagger + b_{iq}\right) I_{\mathrm{TLS}}. \tag{8.28}$$

This shift can be absorbed into the bath Hamiltonian, where (up to a total additive constant) we get

$$\begin{aligned} H_{\mathrm{bath}} &= \sum_{iq}\beta_{iq}\left(b_{iq}^\dagger - \frac{\gamma_q}{\beta_{iq}}\right)\left(b_{iq} - \frac{\gamma_q}{\beta_{iq}}\right) \\ &= \sum_{iq}\beta_{iq}c_{iq}^\dagger c_{iq} \end{aligned} \tag{8.29}$$

with $c_{iq} = \left(b_{iq} - \frac{\gamma_q}{\beta_{iq}}\right)$. This in turn shifts the interaction Hamiltonian, giving an additional term

$$-4\sum_{iq}|e_i\rangle\langle e_i|\frac{\gamma_q^2}{\beta_{iq}}. \tag{8.30}$$

We hence shift each of the qubit energies ϵ_i by an amount $-4\sum_q \frac{\gamma_q^2}{\beta_{iq}}$. We have previously assumed that the (smooth) density of states in frequency space is related to these discrete decay terms as

$$J(\nu) = 2\pi \sum_{iq} \gamma_q^2 \delta(\nu - \beta_{iq}). \tag{8.31}$$

We can thus write

$$\sum_{iq} \frac{\gamma_q^2}{\beta_{iq}} \delta(\nu - \beta_{iq}) = \sum_{iq} \frac{\gamma_q^2}{\nu} \delta(\nu - \beta_{iq}) = \int_{-\infty}^{\infty} \mathrm{d}\nu \, \frac{J(\nu)}{2\pi\nu}, \tag{8.32}$$

which gives an effective system Hamiltonian that depends on frequency:

$$H'_{\mathrm{sys}} = \sum_i \left(\epsilon_i - \int_{-\infty}^{\infty} \mathrm{d}\nu \, \frac{2J(\nu)}{\pi\nu} \right) |e_i\rangle\langle e_i|. \tag{8.33}$$

This is effectively a zero energy Lamb shift. Like the Lamb shift, given a low frequency cutoff the integral is many orders of magnitude smaller than the other energy scales and is hence negligible.

Part IV

Concluding Remarks

Chapter 9

Conclusion

In this thesis we have seen the application of various theoretical tools to collective physics in quantum optics and circuit QED. Our study of the Jaynes-Cummings Hubbard model out of equilibrium compares the results of numerical mean-field decoupling, analytical spin chain and semiclassical models, a Keldysh path integral calculation and the implementation of time-evolving block decimation applied to the density matrix equation of motion.

Additionally, we have studied the dephasing dominated response of several qubits coupled strongly to a single cavity mode. The presence of non-trivial $1/f$ noise in this setting leads to narrowing of the collective Rabi linewdiths as demonstrated by a Bloch-Redfield calculation.

A possible future avenue to pursue in the context of this work may be a more complete analysis of the Jaynes-Cummings Hubbard model within time-evolving block decimation. Starting from the steady state results, one may go on to calculating fluorescence spectra that take into account the actual propagation of perturbances along the chain of cavities. Spatial correlations between cavities may give clues as to the nature of the full system density matrix, in particular regarding the possible existence of bimodal behaviour. Having a tractable matrix product description of the array of coupled cavities also makes it possible to study finite momentum effects. Finally, implementing different pump schemes, such as 'transport measurements' where one end of a chain of cavities is driven and the response of the opposite end is

observed, may yield results that are easy to confirm experimentally.

In the context of non-trivial noise in strongly coupled circuit QED systems it may be interesting to study in more detail the effect of different noise spectra and the possible use of linewidth measurements as a function of detuning for extracting the noise spectra.

Bibliography

[1] F. Nissen, S. Schmidt, M. Biondi, G. Blatter, H. Türeci, and J. Keeling, "Nonequilibrium Dynamics of Coupled Qubit-Cavity Arrays," *Physical Review Letters*, vol. 108, p. 233603, 2012.

[2] G. Kulaitis, F. Krüger, F. Nissen, and J. Keeling, "Disordered driven coupled cavity arrays: Nonequilibrium stochastic mean-field theory," *Physical Review A*, vol. 87, p. 013840, 2013.

[3] F. Nissen, J. M. Fink, J. A. Mlynek, A. Wallraff, and J. Keeling, "Collective suppression of linewidths in circuit QED," *arXiv preprint arXiv:1302.0665*, 2013.

[4] R. Dicke, "Coherence in spontaneous radiation processes," *Physical Review*, vol. 93, no. 1, p. 99, 1954.

[5] K. Hepp and E. H. Lieb, "Equilibrium statistical mechanics of matter interacting with the quantized radiation field," *Physical Review A*, vol. 8, pp. 2517–2525, 1973.

[6] A. D. Greentree, C. Tahan, J. H. Cole, and L. C. L. Hollenberg, "Quantum phase transitions of light," *Nature Physics*, vol. 2, pp. 856–861, 2006.

[7] A. J. Ramsay, A. V. Gopal, E. M. Gauger, A. Nazir, B. W. Lovett, A. M. Fox, and M. S. Skolnick, "Damping of exciton Rabi rotations by acoustic phonons in optically excited InGaAs/GaAs quantum dots," *Physical Review Letters*, vol. 104, p. 017402, 2010.

[8] A. J. Ramsay, T. M. Godden, S. J. Boyle, E. M. Gauger, A. Nazir, B. W. Lovett, A. M. Fox, and M. S. Skolnick, "Phonon-induced rabi-frequency renormalization of optically driven single InGaAs/GaAs quantum dots," *Physical Review Letters*, vol. 105, p. 177402, 2010.

[9] D. Walls and G. Milburn, *Quantum optics*. Springer, 2008.

[10] M. Lax, "Formal theory of quantum fluctuations from a driven state," *Physical Review*, vol. 129, pp. 2342–2348, 1963.

[11] S. Swain, "Master equation derivation of quantum regression theorem," *Journal of Physics A: Mathematical and General*, vol. 2577, 1999.

[12] H. Carmichael, *An open systems approach to Quantum Optics: lectures presented at the Université Libre de Bruxelles, October 28 to November 4, 1991*, vol. 18. Springer, 1993.

[13] R. Dümcke and H. Spohn, "The proper form of the generator in the weak coupling limit," *Zeitschrift für Physik B Condensed Matter*, vol. 34, no. 4, pp. 419–422, 1979.

[14] L. Keldysh, "Diagram technique for nonequilibrium processes," *Zh.Eksp.Teor.Fiz.*, vol. 47, pp. 1515–1527, 1964.

[15] A. Kamenev, "Many-body theory of non-equilibrium systems," pp. 1–71.

[16] M. Szymanska, J. Keeling, and P. Littlewood, "Mean-field theory and fluctuation spectrum of a pumped decaying Bose-Fermi system across the quantum condensation transition," *Physical Review B*, vol. 75, p. 195331, 2007.

[17] J. Maciejko, "An Introduction to Nonequilibrium Many-Body Theory," 2007.

[18] J. Schwinger, "Brownian motion of a quantum oscillator," *Journal of Mathematical Physics*, vol. 2, p. 407, 1961.

[19] J. Keeling, M. Szymanska, and P. Littlewood, "Keldysh Green's function approach to coherence in a non-equilibrium steady state: connecting Bose-Einstein condensation and lasing," in *Optical Generation and Control of Quantum Coherence in Semiconductor Nanostructures* (G. Slavcheva and P. Roussignol, eds.), vol. 0 of *NanoScience and Technology*, pp. 293–329, Springer Berlin Heidelberg, 2010.

[20] S. White, "Density matrix formulation for quantum renormalization groups," *Physical Review Letters*, vol. 69, no. 19, pp. 2863–2866, 1992.

[21] G. Vidal, J. I. Latorre, E. Rico, and A. Kitaev, "Entanglement in quantum critical phenomena," *Physical Review Letters*, vol. 90, p. 227902, 2003.

[22] G. Vidal, "Efficient Classical Simulation of Slightly Entangled Quantum Computations," *Physical Review Letters*, vol. 91, pp. 12–15, 2003.

[23] M. Cazalilla and J. Marston, "Time-Dependent Density-Matrix Renormalization Group: A Systematic Method for the Study of Quantum Many-Body Out-of-Equilibrium Systems," *Physical Review Letters*, vol. 88, p. 256403, 2002.

[24] G. Vidal, "Efficient Simulation of One-Dimensional Quantum Many-Body Systems," *Physical Review Letters*, vol. 93, p. 040502, 2004.

[25] A. J. Daley, C. Kollath, U. Schollwöck, and G. Vidal, "Time-dependent density-matrix renormalization-group using adaptive effective Hilbert spaces," *Journal of Statistical Mechanics: Theory and Experiment*, vol. 2004, p. P04005, 2004.

[26] M. Zwolak and G. Vidal, "Mixed-State Dynamics in One-Dimensional Quantum Lattice Systems: A Time-Dependent Superoperator Renormalization Algorithm," *Physical Review Letters*, vol. 93, p. 207205, Nov. 2004.

[27] E. Schmidt, "Zur Theorie der linearen und nichtlinearen Integralgleichungen," *Mathematische Annalen*, 1907.

[28] R. Orús and G. Vidal, "Infinite time-evolving block decimation algorithm beyond unitary evolution," *Physical Review B*, vol. 78, p. 155117, 2008.

[29] E. Jaynes and F. Cummings, "Comparison of quantum and semiclassical radiation theories with application to the beam maser," *Proceedings of the IEEE*, 1963.

[30] J. Koch, T. M. Yu, J. Gambetta, A. A. Houck, D. I. Schuster, J. Majer, A. Blais, M. H. Devoret, S. M. Girvin, and R. J. Schoelkopf, "Charge-insensitive qubit design derived from the cooper pair box," *Physical Review A*, vol. 76, p. 042319, 2007.

[31] T. Niemczyk, F. Deppe, H. Huebl, E. Menzel, F. Hocke, M. Schwarz, J. J. García-Ripoll, D. Zueco, T. Hümmer, E. Solano, *et al.*, "Circuit quantum electrodynamics in the ultrastrong-coupling regime," *Nature Physics*, vol. 6, no. 10, pp. 772–776, 2010.

[32] A. Imamoḡlu, H. Schmidt, G. Woods, and M. Deutsch, "Strongly interacting photons in a nonlinear cavity," *Physical Review Letters*, vol. 79, pp. 1467–1470, 1997.

[33] C. Lang, D. Bozyigit, C. Eichler, L. Steffen, J. M. Fink, A. A. Abdumalikov, M. Baur, S. Filipp, M. P. da Silva, A. Blais, and A. Wallraff, "Observation of resonant photon blockade at microwave frequencies using correlation function measurements," *Physical Review Letters*, vol. 106, p. 243601, 2011.

[34] L. S. Bishop, J. M. Chow, J. Koch, A. A. Houck, M. H. Devoret, E. Thuneberg, S. M. Girvin, and R. J. Schoelkopf, "Nonlinear response of the vacuum Rabi resonance," *Nature Physics*, vol. 5, pp. 105–109, 2008.

[35] J. Gea-Banacloche, "Collapse and revival of the state vector in the Jaynes-Cummings model: An example of state preparation by a quantum apparatus," *Physical Review Letters*, vol. 65, no. 27, pp. 3385–3388, 1990.

[36] J. Cresser, "Thermal equilibrium in the Jaynes-Cummings model," *Journal of Modern Optics*, vol. 39, no. 11, pp. 2187–2192, 1992.

[37] L. S. Bishop, *Circuit Quantum Electrodynamics*. PhD thesis.

[38] L. Tian and H. J. Carmichael, "Quantum trajectory simulations of two-state behavior in an optical cavity containing one atom," *Physical Review A*, vol. 46, pp. R6801–R6804, 1992.

[39] J. M. Fink, R. Bianchetti, M. Baur, M. Göppl, L. Steffen, S. Filipp, P. J. Leek, A. Blais, A. Wallraff, and M. Go, "Dressed Collective Qubit States and the Tavis-Cummings Model in Circuit QED," *Physical Review Letters*, vol. 103, no. 8, p. 083601, 2009.

[40] M. Born and E. Wolf, *Principles of Optics*. Cambridge University Press, 2005.

[41] J. Eberly and K. Wodkiewicz, "The time-dependent physical spectrum of light," *Optical Society of America, Journal*, vol. 836, no. 1968, pp. 1252–1261, 1977.

[42] J. Keeling, "Light-matter interaction and quantum optics," *Graduate lectures*.

[43] B. Mollow, "Power spectrum of light scattered by two-level systems," *Physical Review*, vol. 188, no. 5, 1969.

[44] J. Koch and K. Le Hur, "Superfluid-Mott-insulator transition of light in the Jaynes-Cummings lattice," *Physical Review A*, vol. 80, p. 023811, 2009.

[45] A. Cottet, *Implementation of a quantum bit in a superconducting circuit*. PhD thesis, Universite Paris VI, 2002.

[46] V. Bouchiat, D. Vion, P. Joyez, D. Esteve, and M. H. Devoret, "Quantum Coherence with a Single Cooper Pair," *Physica Scripta*, vol. T76, no. 1, p. 165, 1998.

[47] A. A. Clerk, M. H. Devoret, S. M. Girvin, F. Marquardt, and R. J. Schoelkopf, "Introduction to Quantum Noise, Measurement and Amplification," *Rev. Mod. Phys.*, 2008.

[48] C. Lang, D. Bozyigit, C. Eichler, L. Steffen, J. Fink, A. Abdumalikov, M. Baur, S. Filipp, M. da Silva, A. Blais, and A. Wallraff, "Observation of Resonant Photon Blockade at Microwave Frequencies Using Correlation Function Measurements," *Physical Review Letters*, vol. 106, pp. 243601, 2011.

[49] D. Bozyigit, C. Lang, L. Steffen, J. M. Fink, C. Eichler, M. Baur, R. Bianchetti, P. J. Leek, S. Filipp, M. P. da Silva, A. Blais, and A. Wallraff, "Antibunching of microwave-frequency photons observed in correlation measurements using linear detectors," *Nature Physics*, vol. 7, pp. 154–158, 2010.

[50] A. Houck, D. Schuster, J. Gambetta, J. Schreier, B. Johnson, J. Chow, L. Frunzio, J. Majer, M. Devoret, S. Girvin, *et al.*, "Generating single microwave photons in a circuit," *Nature*, vol. 449, no. 7160, pp. 328–331, 2007.

[51] J. Fink, M. Göppl, M. Baur, R. Bianchetti, P. Leek, A. Blais, and A. Wallraff, "Climbing the Jaynes–Cummings ladder and observing its nonlinearity in a cavity QED system," *Nature*, vol. 454, no. 7202, pp. 315–318, 2008.

[52] A. J. Hoffman, S. J. Srinivasan, J. M. Gambetta, and A. A. Houck, "Coherent control of a superconducting qubit with dynamically tunable qubit-cavity coupling," *Physical Review B*, vol. 84, p. 184515, 2011.

[53] A. J. Hoffman, S. J. Srinivasan, S. Schmidt, L. Spietz, J. Aumentado, H. E. Türeci, and A. A. Houck, "Dispersive photon blockade in a superconducting circuit," *Physical Review Letters*, vol. 107, p. 053602, 2011.

[54] D. Underwood, W. Shanks, J. Koch, and a. Houck, "Low-disorder microwave cavity lattices for quantum simulation with photons," *Physical Review A*, vol. 86, p. 023837, 2012.

[55] M. P. A. Fisher, P. B. Weichman, G. Grinstein, and D. S. Fisher, "Boson localization and the superfluid-insulator transition," *Physical Review B*, vol. 40, pp. 546–570, 1989.

[56] S. Schmidt and G. Blatter, "Strong Coupling Theory for the Jaynes-Cummings-Hubbard Model," *Physical Review Letters*, vol. 103, p. 086403, 2009.

[57] D. Rossini and R. Fazio, "Mott-insulating and glassy phases of polaritons in 1d arrays of coupled cavities," *Physical Review Letters*, vol. 99, p. 186401, 2007.

[58] J. Zhao, A. W. Sandvik, and K. Ueda, "Insulator to superfluid transition in coupled photonic cavities in two dimensions," *arXiv preprint arXiv:0806.3603v2*, 2008.

[59] M. Aichhorn, M. Hohenadler, C. Tahan, and P. Littlewood, "Quantum Fluctuations, Temperature, and Detuning Effects in Solid-Light Systems," *Physical Review Letters*, vol. 100, p. 216401, 2008.

[60] A. Tomadin, V. Giovannetti, R. Fazio, D. Gerace, I. Carusotto, H. E. Türeci, and A. Imamoglu, "Signatures of the superfluid-insulator phase transition in laser-driven dissipative nonlinear cavity arrays," *Physical Review A*, vol. 81, p. 061801, 2010.

[61] T. Grujic, S. R. Clark, D. Jaksch, and D. G. Angelakis, "Non-equilibrium many-body effects in driven nonlinear resonator arrays," *New Journal of Physics*, vol. 14, no. 10, p. 103025, 2012.

[62] M. Leib and M. J. Hartmann, "Bosehubbard dynamics of polaritons in a chain of circuit quantum electrodynamics cavities," *New Journal of Physics*, vol. 12, no. 9, p. 093031, 2010.

[63] M. J. Hartmann, "Polariton Crystallization in Driven Arrays of Lossy Nonlinear Resonators," *Physical Review Letters*, vol. 104, p. 113601, 2010.

[64] V. N. Popov and S. Fedotov, "The functional integration method and diagram technique for spin systems," *Zh. Eksp. Teor. Fiz.*, vol. 94, no. 3, pp. 183–194, 1988.

[65] R. H. Dicke, "Coherence in spontaneous radiation processes," *Physical Review*, vol. 93, pp. 99–110, 1954.

[66] H. J. Carmichael and D. F. Walls, "Master equation for strongly interacting systems," *Journal of Physics A: Mathematical, Nuclear and General*, vol. 6, no. 10, p. 1552, 1973.

[67] A. J. Ramsay, A. V. Gopal, E. M. Gauger, A. Nazir, B. W. Lovett, A. M. Fox, and M. S. Skolnick, "Damping of Exciton Rabi Rotations by Acoustic Phonons in Optically Excited InGaAs/GaAs Quantum Dots," *Physical Review Letters*, vol. 104, p. 017402, 2010.

[68] A. J. Ramsay, T. M. Godden, S. J. Boyle, E. M. Gauger, A. Nazir, B. W. Lovett, A. V. Gopal, A. M. Fox, and M. S. Skolnick, "Effect of detuning on the phonon induced dephasing of optically driven InGaAs/GaAs quantum dots," *J. Appl. Phys.*, vol. 109, no. 10, p. 102415, 2011.

[69] R. K. Wangsness and F. Bloch, "The dynamical theory of nuclear induction," *Physical Review*, vol. 89, pp. 728–739, 1953.

[70] A. G. Redfield, "Nuclear magnetic resonance saturation and rotary saturation in solids," *Physical Review*, vol. 98, pp. 1787–1809, 1955.